Radiation Effects in Zircon

Rodney C. Ewing

Department of Nuclear Engineering & Radiological Sciences
Department of Materials Science & Engineering
Department of Geological Sciences
University of Michigan
Ann Arbor, Michigan 48109

Alkiviathes Meldrum

Department of Physics
The University of Alberta
Edmonton, Alberta
Canada T6G 2J1

LuMin Wang

Department of Nuclear Engineering & Radiological Sciences
University of Michigan
Ann Arbor, Michigan 48109

William J. Weber and L. René Corrales

Pacific Northwest National Laboratory
P.O. Box 999
Richland, Washington 99352

INTRODUCTION

The widespread distribution of zircon in the continental crust, its tendency to concentrate trace elements, particularly lanthanides and actinides, its use in age-dating, and its resistance to chemical and physical degradation have made zircon the most important accessory mineral in geologic studies. Because zircon is highly refractory, it also has important industrial applications, including its use as a lining material in high-temperature furnaces. However, during the past decade, zircon has also been proposed for advanced technology applications, such as a durable material for the immobilization of plutonium (Ewing et al. 1995) or, when modified by ion-beam irradiation, as an optic waveguide material (Babsail et al. 1991). In all of these applications, the change in properties as a function of increasing radiation dose is crucial (see for example, Lumpkin 2001). In this chapter, we summarize the state-of-knowledge on the radiation damage accumulation process in zircon.

Although the concentrations of uranium and thorium are generally low (typically less than 5,000 ppm) in natural zircon, some zircon crystals are of great age (the oldest dated zircon grains are >4 Ga) and, thus, have calculated doses of $>10^{19}$ α-decay events/g, well beyond the dose required for the radiation-induced transformation to the aperiodic, metamict state. In an α-decay event, the α-particle dissipates most of its energy (4.0 to 6.0 MeV for actinides) by ionization processes over a range of 10 to 20 μm, but undergoes enough elastic collisions along its path to produce approximately one hundred isolated atomic displacements. The largest number of displacements occurs near the end of the α-particle trajectory. The more massive, but lower energy, α-recoil (70 keV ^{234}Th-recoil from decay of ^{238}U) dissipates nearly all of its energy in elastic collisions over only 30 to 40 nm, transferring enough kinetic energy to cause ~1,000 atomic displacements

1529-6466/03/0053-0014$05.00

according to calculations (Weber 1993). This creates a "cascade" of atomic collisions in which the total energy can be as much as 1 eV/atom, and whose structure and evolution can only be modeled by computer simulations. The cascade duration is extremely short ($<10^{-12}$ s), after which displacements by elastic interactions cease and the cascade gradually loses energy as it cools to ambient temperature, typically "quenching" in nanoseconds. During this cooling phase, relaxation and diffusion reduce the number of displaced atoms in the cascade, and the final damage state consists of a small low-density core surrounded by a halo of interstitials (Slater 1951, Brinkman 1954, Trachenko et al. 2002, 2003). A single α-decay event generates approximately 700 to 2,000 "permanently" displaced atoms, significantly more than the 0.1 displacements generated per β-decay event (Weber 1993, Weber et al. 1998). In the decay chain of ^{238}U, there are eight α-decay events; ^{232}Th has six. Because of the large number of atomic displacements during an α-decay event, the accumulation and overlap of the individual cascades, as well as the presence of still crystalline but highly-strained domains, has a profound effect on the structure and properties of the damaged solid. In the case of zircon, there is a dramatic decrease in density (17%), a decrease in birefringence until isotropic, a decrease in the elastic moduli (69%), a decrease in hardness (40%), an increase in fracture toughness (Chakoumakos et al. 1987, Chakoumakos et al. 1991) and an increase in dissolution rate of one to two orders of magnitude (Ewing et al. 1982). Over extended time, the final damage microstructure is both time and temperature dependent because of annealing and recrystallization of damaged and strained domains (Weber et al. 1997).

Zircon figured prominently in the earliest studies of the metamict state and radiation damage (see Ewing 1994 for a summary of this early history). Stackelberg and Rottenbach (1940) had noted changes in density, refractive indices and birefringence with increasing α-decay dose and even tried to test this hypothesis by irradiating a thin slab of zircon with α-particles, perhaps the first ion-beam modification experiment. Still, metamict minerals remained a mineralogical oddity for several decades, until the systematic review of radiation-induced property changes by Pabst (1952) in his Presidential Address to the Mineralogical Society of America. Early studies of the helium method for age determination (Hurley and Fairbairn 1952) led to the idea that radiation-damage accumulation could be used for age-dating minerals. Hurley and Fairbairn (1953) completed the first systematic study of a suite of increasingly damaged zircon crystals and quantified the amount of damage based on X-ray diffraction data. This paper is remarkable, as it relates their results for zircon to the new field of radiation damage in reactor materials and draws heavily on what was known at that time about the physics of the radiation damage process. Although their interpretation was limited by a lack of experimental data (e.g., they estimated that 5,000 atoms were permanently displaced by each α-decay event), their approach was sound and laid the foundations of the work that continues today. Holland and Gottfried (1955) completed a classic study of the effects of α-decay events on density, optical properties and unit cell parameters as determined by X-ray diffraction. Their paper remained a standard reference for the effects of radiation on silicates, but further advances in knowledge had to await the development of more controlled irradiation experiments. Accelerated damage techniques, including doping with extremely short-lived actinides that transmuted by α-decay, such as ^{238}Pu with a half-life of 87.7 years (Exarhos 1984, Weber 1991, Weber et al. 1994, Burakov et al. 2002, Burakov et al. in press), neutron irradiation (Crawford and Wittels 1956, Hayahshi et al. 1990) and ion beam irradiation (Cartz and Fournelle 1979, Wang and Ewing 1992a,b; Ewing et al. 2000) were used to great advantage in simulating the α-decay event damage in natural zircon. We now have experimental data from irradiation experiments with dose rates that vary by more than fifteen orders of magnitude (displaced atoms/s) over a range of temperature from –260 to 800°C (Meldrum et al. 1999a). Based on the studies summarized in this chapter, one can safely state that there is no other mineral or complex ceramic for which there is so much information on the process and effects of radiation damage.

During the 1990s, there has been a small "explosion" of work on radiation damage effects in ceramics in general, and specifically on zircon (Ewing et al. 2000). The experimental work is of

three types:

1. Natural zircon crystals. In these studies, there is generally no lack of material and a wide variety of analytical techniques may be used; however, the conclusions of these studies are always limited by a lack of knowledge of the thermal history of the samples.
2. ^{238}Pu-doped synthetic zircon. These studies are generally conducted under ambient conditions, followed by thermal annealing studies. These are long-term studies, lasting several decades, and the results for only a few samples of longer-term experiments are just now available. Because of restrictions on handling Pu-bearing samples, analytical studies have been limited to simple density determinations, structural analysis using X-ray diffraction, electron microprobe analysis and some spectroscopic studies.
3. Ion-beam irradiated zircon. In these studies, both heavy- and light-ion irradiations have been completed at precisely controlled temperatures. Although the physics of the damage process allows one to correlate the results to α-decay damage, the experimental configuration has limitations. *In situ* irradiations combined with high resolution electron microscopy allow one to observe changes in the atomic-scale structure in real time and determine the dose at which the material becomes amorphous as a function of temperature; however, the high surface area to volume ratio of the thin wedge of the electron transparent region may affect the damage accumulation process as defects migrate to the surface. Most recently, bulk irradiations, followed by examination of samples cut perpendicular to the surface (parallel to the trajectory of the ion), allow one to follow damage effects because the amount of damage varies along the trajectory of the implanted ion. These samples are generally examined by high-resolution transmission electron microscopy (HRTEM) (Lian et al. 2001; Lian et al. in press) or utilize surface techniques, such as X-ray photoelectron spectroscopy (XPS) (Chen et al. 2002). Such studies are time consuming, but can provide critical information on oxidation states, defect formation and migration mechanisms.

Finally, during the past five years, there has been an increased effort to simulation cascade formation and the evolution of the damage microstructure. Computational limitations currently restrict such dynamic calculations to cells that contain less than 400,000 atoms and time periods for cascade evolution of up to 20 picoseconds. The future challenge is in designing experiments and simulations that can be used to test the various models of damage accumulation.

In this chapter, we first review the experimental results for radiation-damaged zircon. We explicitly focus on displacement damage that results from α-decay event cascade formation. The experimental results are then discussed in terms of the different models that have been used to describe the damage accumulation process. The next section summarizes the recent results of computer simulations of atomic-scale processes during the damage process. Despite the substantial progress of the last decade, many questions remain, and these are discussed in the last section.

EXPERIMENTAL RESULTS

We have organized the discussion of experimental results according to the length-scale sampled by each technique. We begin with a discussion of changes in bulk properties, then long-range effects (10 to 100 nm) that capture the changes in the connectivity of the coordination polyhedra, as well as the presence of domains of different structures (e.g., periodic, strained periodic, and aperiodic). Finally, we discuss short-range effects (<1 nm) that reflect changes in the nearest-neighbor coordination geometries. Although this is a convenient and revealing means of following the damage accumulation process, the changes in structure of the damaged material occur at all length-scales simultaneously. No single technique can provide a clear picture of this heterogeneous transition as it occurs over the entire range of dose (Salje et al. 1999). Even a single technique, such as X-ray diffraction, will provide different types of data, e.g., Bragg diffraction maxima from the periodic domains and a diffuse scattering component from interstitial defects and amorphous domains.

Several different units are used to measure the radiation dose, depending on the type of ex-

periment. In studies of naturally damaged or Pu-doped zircon, the age and actinide concentration are used to calculate the dose; whereas, in ion beam experiments, the radiation fluence (ions/cm^2) is measured. In order to compare the amount of damage in natural, Pu-doped, and ion-irradiated zircons, these measurements are converted to a radiation dose, in units of displacements-per-atom (dpa). To convert the fluence to units of dose, a simple formula is used:

$$D_{dpa} = JF/n \quad (1)$$

where D_{dpa} is dose in dpa, J is the number of atomic displacements caused by each ion per unit depth, F is the fluence, and n is the atomic density. J depends on a variety of parameters, including incident ion mass and energy and the displacement energy (E_d) of the target atoms. Monte Carlo computer simulations are used to estimate J. The number of displacements per ion varies inversely with E_d (i.e., the higher the displacement energy, the fewer displacements are caused by each incident ion).

Atomic displacement energies are known for only a relatively few ceramic materials, most of which are simple oxides such as Al_2O_3, MgO, ZnO, CaO, and UO_2 (Zinkle and Kinoshita 1997). Displacement energies generally range from 10 to 70 eV. For example, in Al_2O_3, the typically used displacement energies are 20 eV for Al and 50 eV for oxygen. More recently, molecular dynamics simulations have extended the range of materials for which E_d can be estimated to more complex materials. For zircon, E_d is 89 eV (Zr), 48 eV (Si), and 28 eV (O) (Park et al. 2001).

In order to make quantitative comparisons of the amount of radiation damage in natural and ion-beam-irradiated specimens, the measured concentration of U and Th is also converted to a displacement dose. This can be done in two steps:

$$D_\alpha = 8\,N_{238}[\exp(t/\tau_{(238)}) - 1] + 7\,N_{235}[\exp(t/\tau_{(235)}) - 1] + 6\,N_{232}[\exp(t/\tau_{(232)}) - 1] \quad (2)$$

where D_α is the dose in units of α-decays/g, N_{238}, N_{235}, and N_{232} are the measured number of atoms/g of ^{238}U, ^{235}U, and ^{232}Th, $\tau_{(238)}$, $\tau_{(235)}$, and $\tau_{(232)}$ are their respective half-lives, and t is the geologic age. Studies of radiation damage in minerals usually report D_α. To convert to a dose in dpa:

$$D_{dpa} = \frac{D_\alpha WN}{aA} \quad (3)$$

where A is Avogadro's number, W is the molecular weight of the mineral, n is the average number of displacements per α–decay, and a is the number of atoms per formula unit. The n term is analogous to J in Equation (1) and can be obtained by using the computer simulation (which requires a value for E_d). An advantage to using dpa as the unit of dose is that variations in the displacement energy, E_d, affects Equations (1) and (3) in exactly the same way, so that quantitative comparisons between ion-irradiated and α-decay-damaged materials may be made. The observed amount of disorder may also depend on the flux; however, the calculated number of displacements per atom is independent of this parameter.

Bulk properties

Density. The variation in density as a function of α-decay event dose is important because this relationship is used to distinguish among the different models of damage accumulation mechanism. The effects of increasing damage on the density of natural zircon crystals from Sri Lanka (~570 Ma) have been carefully measured in several papers (e.g., Holland and Gottfried 1955, Murakami et al. 1991). The density decreased by 17% from ~4.7 to 3.90 g/cm^3 at a dose of 10^{19} α-decays/g. The rate of change in density is sigmoidal: i.e., the change is slow at low doses, followed by a more rapid

decrease between 2 to 8×10^{18} α-decays/g, and finally approaching a saturation value of 3.9 g/cm^3 at doses greater than 8×10^{18} α-decays/g.

Weber (1990) reported density measurements for synthetic zircon doped with 8 mol % ^{238}Pu ($Pu_{0.08}Zr_{0.92}SiO_4$). This zircon showed a more rapid density decrease at doses below ~6×10^{18} α-decays/g than natural zircon. The density of the Pu-substituted zircon saturated at approximately 4.0 g/cm^3. The shallower initial density decrease in natural zircon was attributed to the effects of thermal recovery over geologic time of damaged, but not yet amorphous material (Weber 1990, Murakami et al. 1991). The overall density of Pu-doped zircon decreased by 14.1% before reaching saturation, as compared to a decrease of 15.6% for natural zircon (Weber 1990).

Weber (1990) and Murakami (1991) described dose-dependent density decrease by:

$$\Delta\rho/\rho = A[1 - \exp(-(BD)^n)] \quad (4)$$

where $\Delta\rho/\rho$ is the density change normalized to the density of the initially crystalline zircon, A is the relative density change at saturation, B is the mass of material damaged per α-decay event, D is the α-decay dose, and n is an "order parameter" that gives the sigmoidal shape to the curve. B was found to be approximately 2-3 $\times 10^{-19}$g, corresponding to a total of 4,000-6,000 atoms of "damaged material" per α-decay event (this number is greater than the calculated number of displaced atoms, because the "damaged" volume is the affected volume per α-decay event that contains all the damage, defects and amorphous domains). The order parameter has values between 1.7-2.3 (Weber 1990, Murakami et al. 1991), but the order parameter has no specific physical meaning. Weber et al. (1994) expressed the normalized macroscopic volume swelling $\Delta V_m/V_0$ as:

$$\Delta V_m/V_0 = f_c\Delta V_{uc}/V_0 + f_a\Delta V_a/V_0 \quad (5)$$

in which $\Delta V_{uc}/V_0$ is the normalized unit-cell volume of the crystalline phase, $\Delta V_a/V_0$ is the normalized volume of amorphous zircon, f_c is the mass fraction of crystalline zircon, f_a is the mass fraction of amorphous zircon, and V_0 is the normalization parameter (i.e., macroscopic or unit-cell volume of undamaged zircon). In order to apply this equation to obtain the dose dependence of the amorphous fraction (f_a), the unit-cell swelling is measured by X-ray diffraction (Weber et al. 1994). Recently, Trachenko et al. (2003) have modeled the volume expansion as a percolation phenomena with a discontinuity in the swelling curve at the percolation threshold.

Optical. Crystalline zircon is uniaxial (refractive indices $n_\varepsilon = 1.984$ and $n_\omega = 1.924$), whereas, amorphous zircon is optically isotropic (Holland and Gottfried 1955). Both indices are independent of dose up to ~2×10^{18} α-decays/g, after which the refractive indices decrease with dose until they saturate at $n_\varepsilon = n_\omega = 1.81$. The very regular decrease in birefringence can be used to estimate the α-decay event dose (Chakoumakos et al. 1987) and the related change in density (Sahama 1981). A careful correlation of electron microprobe analyses of U- and Th-content to calculated dose shows a linear relationship to birefringence (Palenik et al. in press).

Mechanical. Özkan (1976) measured a 69% decrease in the elastic modulus and a 7% decrease in Poisson's ratio for a heavily damaged zircon crystal ($\rho = 3.994$ g/cm^2). The longitudinal and shear elastic moduli decreased with increasing radiation dose reaching saturation values of 1.5 $\times 10^{12}$ and 0.49×10^{12} dyne/cm^2, respectively. Chakoumakos et al. (1991) measured a 40% decrease in hardness and 29% decrease in the elastic modulus (using a nano-indenter for a 275 nm indentation depth) in a zoned zircon where the maximum dose was 10^{19} α-decays/g. The radiation "softening" was accompanied by an unmeasured increase in fracture toughness. This was spectacularly evident in the distribution of fractures in a highly zoned zircon in which fractures in the low dose zones did not propagate across the high-dose zones (Chakoumakos et al. 1987, Chakoumakos et al. 1991). The decreases in hardness (70%) and elastic modulus (42%) were confirmed by nano-indenter measurements of Pb-implanted (540 keV) zircon at doses of 10^{13} to 10^{14} Pb/cm^2 (Oliver et al.

1994). Prior to the radiation "softening"; however, there was a slight increase in hardness (11%) up to a dose of 10^{13} Pb/cm^2. Lee and Tromp (1995) modeled the distribution of fractures in zoned zircon accounting for the changes in mechanical properties and the stresses that result from the volume expansion of the highly damaged zones.

Thermal. The thermal conductivity of zircon decreases by ~25% with increasing dose, due to phonon scattering at α-decay-induced defects (Crawford 1965). In a very preliminary study Raychaudhuri et al. (1980) has shown that metamictization leads to thermal conductivity values comparable to those of other disordered solids.

Chemical durability. Crystalline zircon is stable to such an extent that the equilibrium concentrations of dissolved Zr and Si are on the order of 10^{-9} moles/L (0.1 ppb) at 25°C (Tole 1985). Dissolution of highly damaged zircon follows a first-order reaction, based on Si concentrations. Concentrations of Zr remain below 0.05 ppm (the instrument detection limit) due to precipitation of ZrO_2 and $ZrSiO_4$ (Tole 1985). The leach rate of zircon increases with α-decay damage by one to two orders of magnitude (Ewing et al. 1982). Recently, a high-temperature Soxhlet extractor was designed to measure the forward rate of dissolution of zircon in the range of 120 to 250°C (Helean et al. 1999). The measured rates are as follows: 4.1×10^{-4} (g)(m^{-2})(day^{-1}) at 250°C, 1.7×10^{-4} g·m^{-2}day^{-1} at 200°C and 7.1×10^{-5} g·m^{-2}day^{-1} at 120°C. Using the same experimental technique, Gong et al. (in preparation) completed leaching experiments on highly damaged zircon over the temperature range of 150 to 250°C and measured a three order of magnitude increase in normalized mass loss based on silicon concentrations in solution. The effect of radiation damage on the chemical durability of zircon has also been demonstrated in a field study on the weathering of zircon in detrital sediments of the Amazon Basin (Balan et al. 2001). Their results demonstrate a dramatic decrease in chemical durability at doses greater than 3.5×10^{18} α-decays/g. This is higher than the dose at the first percolation point (2×10^{18} α-decays/g, Ríos et al. 2000a), the point at which the aperiodic domains become fully connected to one another (approximately 30-40% of the total volume is amorphous). When the amorphous domains become interconnected the transport properties of zircon change and both loss of elements by diffusion and bulk dissolution proceed rapidly (Jonckheere and Gögen 2001).

Long range order

X-ray diffraction. The sharp Bragg X-ray diffraction maxima associated with long-range periodicity show a pronounced decrease in intensity and shift to lower values of 2θ with increasing α-decay event dose (Holland and Gottfried 1955, Murakami et al. 1991). The intensity decrease is rapid at low doses, followed by a more gradual dose-dependent decrease until the Bragg diffraction maxima are no longer evident (e.g., Pabst 1952, Holland and Gottfried 1955, Pellas 1965, Vance and Anderson 1972, Weber 1990, Weber et al. 1994; see Fig. 1). A similar effect is observed in ion-irradiated (3 MeV Ar^+) synthetic zircon (Karioris et al. 1982). Holland and Gottfried (1955) observed a complete loss of Bragg diffraction intensity at a dose of 10×10^{18} α-decays/g, for the Sri Lanka zircon.

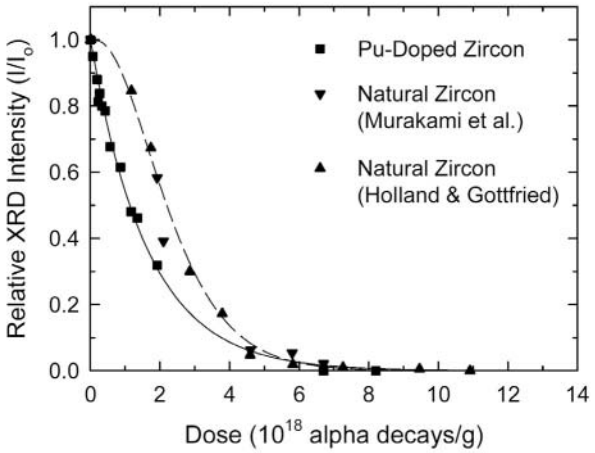

Figure 1. Relative XRD intensities in Pu-doped and natural zircons. [Used by permission of the Materials Research Society, from Weber (1990) *Journal of Material Research*, Vol. 5, Fig. 1, p. 2689.]

Weber (1990) found that after reaching a dose of 6.7×10^{18} α-decays/g, the Pu-substituted zircon was X-ray diffraction amorphous. For both natural and Pu-doped zircon, the decrease in diffraction intensity followed an exponential of the form:

$$I/I_0 = \exp(-BD) \quad (6)$$

where B is, again, the mass of material damaged per α-decay event and D is the α-decay dose. The best fit was obtained for $B = 6.12 \times 10^{-19}$ g for Pu-doped zircon and $B = 6.71 \times 10^{-19}$ g for natural zircon (Weber 1990). The earlier data of Holland and Gottfried (1955) and Murakami et al. (1986) are offset at low dose with respect to Pu-doped zircon (Fig. 1), suggesting a so-called "incubation" dose for natural zircon (Weber 1990, Weber et al. 1994). This offset could be due to thermal recovery of lightly damaged regions or point defects over geologic time.

Murakami et al. (1986, 1991) reported detailed X-ray powder diffraction measurements from a suite of Sri Lanka zircon specimens. Three distinct damage stages were identified. At doses below 3×10^{18} α-decays/g, the initially narrow and intense Bragg maxima decreased by a factor of ~2 and were shifted to slightly lower 2θ, but they remained sharp. This was attributed to the combined effects of unit-cell expansion and strain fields surrounding the expanding damaged regions. In the second stage, which occurs at higher damage levels, the intensity of the Bragg maxima decreased by several orders of magnitude, and the intensity of the diffuse scattering component on the high-2θ side of the Bragg maxima increased substantially. The Bragg maxima at this stage were weak, skewed, and broadened. In the third stage ($>8 \times 10^{18}$ α-decays/g) there was no trace of Bragg diffraction maxima. The dose for the complete disappearance of the Bragg maxima depends on the sensitivity of the experiment for detecting crystalline remnants, but the value of 8×10^{18} α-decays/g obtained by Murakami et al. (1991) has since been confirmed by Ríos et al. (2000a).

The unit-cell parameters were determined by refinement of the X-ray diffraction data. This is more reliably accomplished for low α-decay doses, when the Bragg peaks are still sharp; at higher doses the error in the unit cell parameters is large (Murakami et al. 1991). Several authors have observed that in natural zircon, the net expansion is greater along the *c*-axis than along the *a*-axis, and that there is a significant suppression of unit-cell expansion along the *a*-axis at low doses (Holland and Gottfried 1955, Weber 1990, Murakami et al. 1991, Biagini et al. 1997, Ríos et al. 2000b). The ZrO_8 polyhedra are particularly susceptible to volume expansion with increasing α-decay dose, and since they are isolated from one another along the *c*-axis, the structure can expand more freely along this direction (Ríos et al. 2000b). Furthermore, recrystallization is more efficient parallel to the *a*-axis due to tilting of coordination polyhedra around corner-sharing links (Ríos et al. 2000b). In contrast, the rate of lattice expansion was similar along the *a*- and *c*-directions for both Pu-doped (Weber 1990) and neutron-irradiated (Crawford and Whittles 1952) zircon, and in both cases, there was no suppression of the expansion along the *a*-axis, suggesting preferential recovery parallel to the *a*- axis over geologic time for natural zircon.

The increase in amorphous fraction (f_a) as a function of dose is an important relationship that distinguishes the different models of damage accumulation. Weber (1990) and Weber et al. (1994) combined the X-ray diffraction data with the macroscopic swelling data to estimate the relationship between f_a and dose, using Equation (5). They assumed that (i): $V_a/V_0 = 16.6\%$ (the observed macroscopic swelling of Pu-substituted zircon at saturation), (ii) $f_a + f_c = 1$, and (iii): $\Delta V_m/V_0$ is simply the measured dose-dependent volumetric swelling. The unit-cell expansion ($\Delta V_{uc}/V_0$) was then obtained from the measured shift in the Bragg diffraction maxima. The amorphous fraction obtained with this method varied sigmoidally as a function of α-decay dose (Fig. 2). By plotting the unit-cell and macroscopic swelling independently, Weber (1990) also demonstrated that the volume expansion at low doses is due mostly to unit-cell expansion, but at higher doses the contribution from amorphous zircon dominates. A similar analysis for the Sri Lanka zircon was performed on the data of Holland and Gottfried (1955), with similarly sigmoidal results (Weber 1990, Weber et al. 1994).

However, the curves were offset by ~10^{18} α-decays/g with respect to the Pu-doped zircon (Fig. 2), a fact that was attributed to long-term thermal recovery of lightly damaged zircon under geologic conditions.

Murakami et al. (1991) proposed that there is not a single structure for amorphous zircon, but instead, they observed that the density of aperiodic zircon continued to decrease with increasing α-decay dose even after the sample was X-ray diffraction amorphous. This may result from the fact that the X-ray diffraction of amorphous zircon still contained a substantial crystalline fraction. This observation has since been confirmed by Ríos et al. (2000a) who showed that even the highly damaged zircon still had a crystalline component. Thus, the density of the sample depends on the structure of the crystalline and amorphous domains and the proportion of amorphous to crystalline material, all of which change with dose. At doses below 2 × 10^{18} α-decays/g, the diffuse scattering is shifted to larger diffraction angles and originates from the "compressed" crystalline domains due to the expansion of the damaged domains (Ríos and Salje 1999, Ríos et al. 2000a). At these low doses, macroscopic swelling is dominated by the unit-cell expansion, which also compresses the still-isolated amorphous zones. At this stage, radiation damage produces mainly shear waves in the crystal lattice whose signature is a non-isotropic diffuse scattering around the main Bragg peaks (Ríos and Salje 1999). At higher doses, the amorphous domains become interconnected, the amount of residual crystalline material diminishes, and the amorphous structure is free to swell to its maximum value of ~18%.

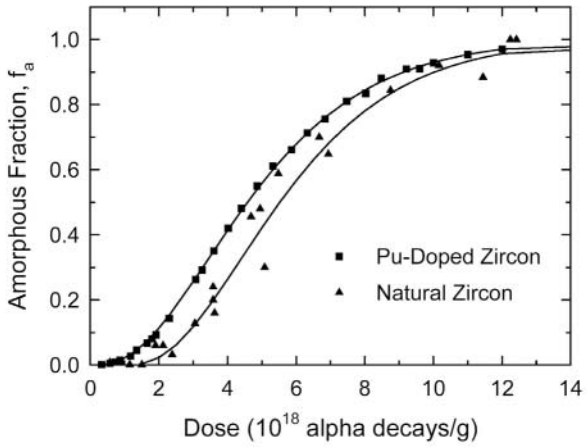

Figure 2. Amorphous fraction, f_a, as a function of dose in Pu-doped and natural zircons. [Used by permission of the Materials Research Society, from Weber (1990) *Journal of Material Research*, Vol. 5, Fig. 12, p. 2695.]

The X-ray diffraction and macroscopic swelling data have been interpreted in terms of a structure consisting of percolating crystalline or amorphous domains (Salje et al. 1999, Ríos et al. 2000a). At low α-decay doses, isolated amorphous regions accumulate and, as the dose increases, they gradually become interconnected.

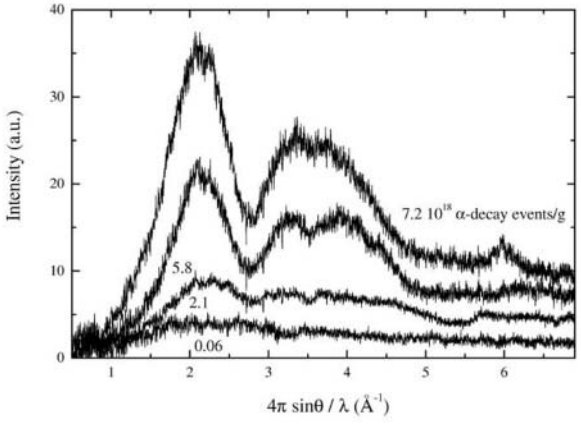

Figure 3. Diffractograms of zircon samples (from the bottom to the top) 4403, 4303, 4304 and 3107. The numbers in the figure indicate the corresponding doses in units of 10^{18} α events/g. For the first three samples any contribution from crystalline areas has been removed. For the last sample (3017), which has a high degree of radiation damage, crystalline area could still be seen, as the peak at 6 Å^{-1} demonstrates. Notice the background increase with the increasing dose. [Used by permission of the Institute of Physics Publishing, Inc., from Ríos et al. (2000a) *Journal of Physics: Condensed Matter*, Vol. 12, Fig. 5, p. 2408.]

Below this first "percolation point" (2×10^{18} α-decays/g for the Sri Lanka zircon) the swelling of amorphous domains is negative due to the expansion of the crystalline structure. The second percolation point is reached below 8×10^{18} α-decays/g, at which point the crystalline regions no longer percolate, and the swelling begins to approach the maximum of 18%. Between the percolation points, amorphous domains can be densified or expanded, depending on the local environment.

Ríos et al. (2000a) used a highly sensitive 7-circle, single-crystal X-ray diffractometer to obtain precise data to estimate the amorphous fraction as a function of α-decay dose (Fig. 3). The amorphous fraction was obtained directly from the X-ray diffraction results by comparing scattering intensities to those from crystalline and amorphous reference specimens:

$$f_a = (I - I_{cryst})/I_{am} \quad (7)$$

where I is the diffuse scattering intensity from the specimen in question, and I_{cryst}, and I_{am} are the intensities obtained from undamaged and X-ray diffraction amorphous zircon, respectively. The background and the Bragg reflections were subtracted and the intensity was integrated at values of $4\pi\sin\theta/\lambda > 5$ Å^{-1}. The resulting amorphous fraction for a suite of Sri Lanka zircon crystals is plotted in Figure 4. The important observations are: (1) there is no offset at low does (i.e., no "incubation" dose); and (2) the curve is not sigmoidal. The line fit is the solution to Equation (6) with $B = 2.7 \times 10^{-19}$ g. The direct increase of f_a with dose is different than the more sigmoidal curve obtained using macroscopic swelling data (Weber 1990, Murakami et al. 1991, Weber et al. 1994). In fact, Ríos et al. showed that that V_a/V_0 in Equation (5) is not constant but depends on the degree of damage, so that previous assumptions used to generate the dose dependence of the amorphous fraction may not have been strictly valid.

Neutron diffraction. There is one neutron diffraction study of a ^{238}Pu-doped zircon that has reached a dose of 2.8×19^{19} α-decays/g, nearly three times the dose required to fully amorphize zircon (Fortner et al. 1999). No evidence of residual microcrystallinity was found. The pair-distribution function indicated that the fully amorphous zircon had the structure of an oxide glass with the structural units of zircon largely preserved and little phase separation.

Transmission electron microscopy (TEM). The first systematic TEM study of radiation effects in zircon as a function of increasing α-decay dose was completed by Bursill and McLaren (1966). They confirmed the three stage model of damage accumulation (Holland and Gottfried 1955) that was based on x-ray diffraction data; however, they showed that zircon at Stage III of the

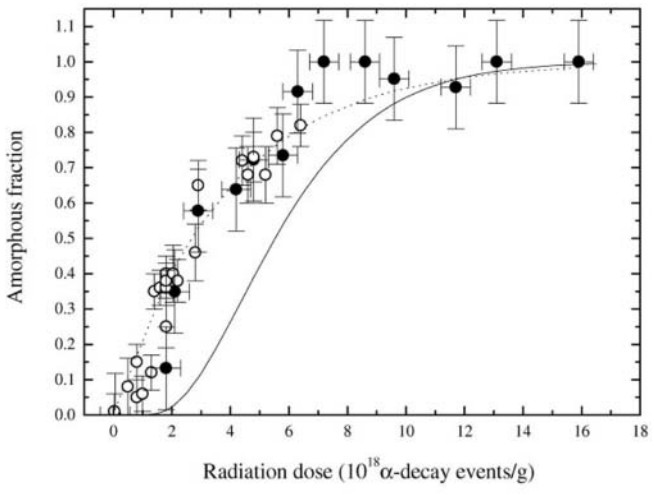

Figure 4. Amorphous fraction, f_a^{exp}, in various zircon samples versus radiation dose. Full circles represent the experimental data as determined following the expression given in Ríos et al. (2000a); the dotted line show the best fit obtained using the direct amorphization model. Open circles indicate data from infrared spectroscopy. The continuous line is the f_a obtained from an equation by Weber (1993). The error bars for the dose are estimated to be about $\pm 0.5 \times 10^{18}$ α-decay events/g. [Used by permission of the Institute of Physics Publishing, Inc., from Ríos et al. (2000a) *Journal of Physics: Condensed Matter*, Vol. 12, Fig. 6, p. 2409.]

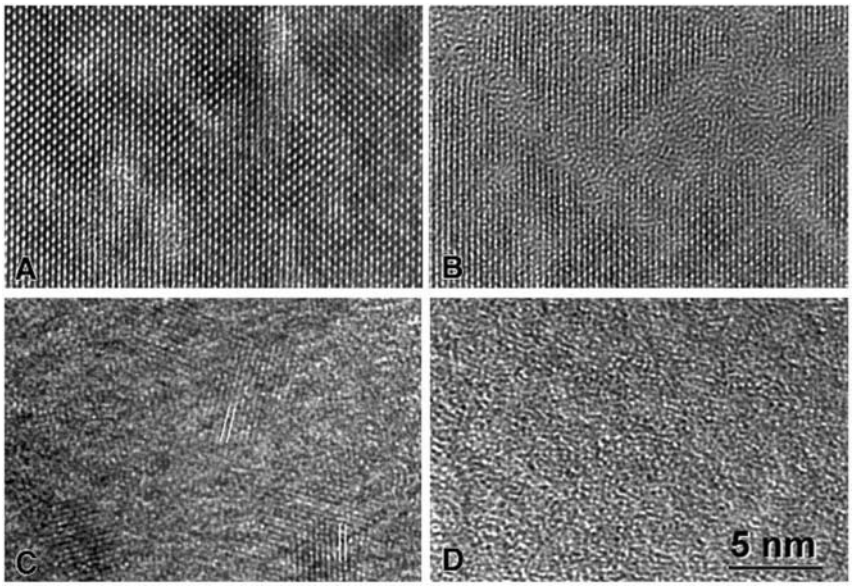

Figure 5. HRTEM micrographs of self-radiation damage in natural zircons showing increased degree of amorphization with increasing dose: (a) 0.0025 dpa; (b) 0.091 dpa; (c) 0.32 dpa; (d) 0.50 dpa. The spacing marked in (c) is 0.33 nm (the (200) d-spacing). The slight rotation of the remaining crystallites in the amorphous matrix in (c) is caused by local strain fields induced by amorphization. [Used by permission of the Materials Research Society, from Weber et al. (1994) *Journal of Material Research*, Vol. 9, Fig. 2, p. 690.]

damage state (apparently amorphous as determined by X-ray diffraction) actually consisted of slightly misoriented crystallites of "normal" zircon approximately 10 nm in size. They also identified small amounts of ZrO_2 in highly damaged zircon. On annealing, voids or bubbles formed (probably of He) in one sample, as well as dislocation loops on {101}, due to the condensation of point defects. Subsequent TEM studies (Headley et al. 1981, 1982b; Yada et al. 1981, 1987; Murakami et al. 1991, Weber et al. 1994, Palenik et al. in press) confirmed the evolution of the microstructure with increasing α-decay event damage. A typical sequence is shown in Figure 5. At very low doses (>0.01 dpa), zircon shows no evidence of damage and has a well-defined atomic-scale periodicity. At a low α-decay dose (0.01 to 0.3 dpa), regions (2-5 nm) of mottled diffraction contrast occur. With increasing α-decay dose, lattice fringe-free areas of mottled diffraction contrast become more numerous and interconnected, and at a still higher dose (> 0.3 dpa), the microstructure consists of crystalline islands in an aperiodic matrix. These crystallites are rotated by up to 15° with respect to the original lattice orientation. Above 0.5 dpa (10^{19} α-decays/g), the zircon appears to be fully aperiodic, as evidenced from electron diffraction and HRTEM imaging.

Although there is a long history of the use of ion beam irradiations to simulate the α-decay and fission track damage effects in zircon (Cartz and Fournelle 1979, Karioris et al. 1981, Headley et al. 1982a, Petit et al. 1987, Bursill and Braunshausen 1990), Wang et al. (1991, 1993) and Wang and Ewing (1992a) were the first to complete *in situ* TEM studies of amorphization of zircon during an ion beam irradiation, using the HVEM-Tandem Facility at Argonne National Laboratory (Wang 1998). This facility consists of a modified 1 MeV electron microscope interfaced with a 2 MeV tandem ion accelerator that allowed *in situ* observation of the sample over a wide range of temperatures (Ewing et al. 2000). The initial irradiations were with 700 and 1500 keV Kr^+, 1500 keV Xe^+ and 400 keV He^+ (Wang and Ewing 1992a). The evolution of electron-diffraction patterns with increasing dose is comparable in many respects with the X-ray diffraction and TEM results for natural zircon (Murakami et al. 1991, Weber et al. 1994). At low to intermediate doses (< 0.2 dpa), the higher-order maxima become fainter and a diffuse diffraction "halo" develops around the trans-

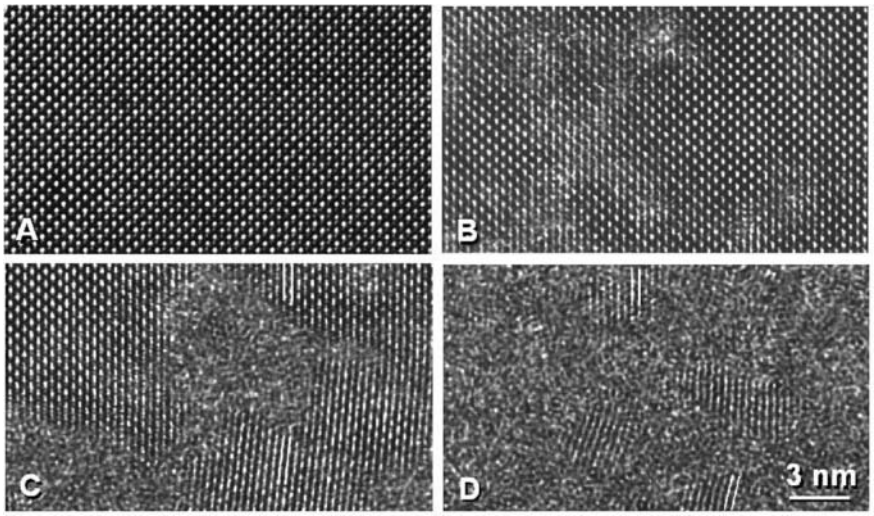

Figure 6. HRTEM images of crystalline to amorphous transformation in synthetic zircon irradiated with 1.5 MeV Kr^+ ions at 300 K: (a) unirradiated; (b) 0.057 dpa; (c) 0.17 dpa; (d) 0.34 dpa. Complete amorphization was achieved at 0.55 dpa. The spacing marked in (c) and (d) is 0.33 nm (the (200) d-spacing). Note the similarity of the images in (b), (c), and (d) with those for self-radiation damage of natural zircon in Figs. 5(a), (b), and (c). [Used by permission of the Materials Research Society, from Weber et al. (1994) *Journal of Material Research*, Vol. 9, Fig. 8, p. 694.]

mitted beam. At higher doses (0.2 to 0.5 dpa), the diffuse scattering becomes stronger, the higher-order maxima disappear entirely, and the remaining electron-diffraction maxima show an arc-like appearance characteristic of crystallites that are slightly rotated (e.g., Headley et al. 1981, Wang and Ewing 1992a, Weber et al. 1994, Meldrum et al. 1999a). At still higher doses (> 0.5 dpa), all of the diffraction maxima disappear, leaving the transmitted beam and the diffuse diffraction halo as the only remaining features in the electron-diffraction patterns. High-resolution TEM images of the fully-damaged zircon confirm the complete loss of lattice fringes. A sequence of high-resolution images of zircon irradiated with 1.5 MeV Kr^+ is shown in Figure 6 (Weber et al. 1994). The overall microstructural evolution with increasing ion dose closely parallels that of α-decay damage in natural zircon. Weber et al. (1994) found that the amorphization dose of the ion-irradiated zircon (0.55 dpa) was similar to that α-decay-amorphized zircon (0.50 dpa). In a later study (Weber et al. 1999), an even lower amorphization dose (0.30 dpa) was determined for ion-irradiated zircon.

Numerous *in situ* ion beam irradiations studies have now been completed on zircon (see summary by Ewing et al. 2000). Although ion beam irradiation reproduces the microstructure of α-decay damaged zircon under controlled temperature conditions, there are a number of experimental limitations. The high surface area to irradiated volume ratio in the electron-transparent region of the sample may affect the damage accumulation process, that is isolated defects migrate and are annihilated at the surface. The electron beam may cause radiation-enhanced migration of defects; thus, increasing the dose required for amorphization. Finally, the dose rates for the ion beam irradiations are many orders of magnitude greater than that for natural or Pu-doped zircon. The first two limitations can be overcome by bulk irradiations of zircon followed by cross-sectional HRTEM analysis. These studies are now in progress. There are also important limitations related to the HRTEM technique. In a systematic study of simulated images of mixed crystalline and aperiodic domains, Miller and Ewing (1992) demonstrated that there can be a substantial fraction (up to 20%) of aperiodic material (e.g., isolated cascades in a crystalline matrix) present, but not evident in the high-resolution TEM image. Depending on the thickness of the examined region, the crystalline fraction dominates the HRTEM image. Based on the simulated images, a single α-recoil cascade should

have an apparent diameter of less than 4.0 nm. These calculations confirm that TEM studies cannot provide a quantitative estimate of the amorphous fraction. Zircon that appears completely amorphous by HRTEM/selected area electron diffraction (SAED) still retains evidence of residual atomic-scale order. Murakami et al. (1991) observed textured or braided regions in electron-diffraction amorphous zircon. Nasdala et al. (2002a,b) used image processing techniques to highlight the presence of discontinuous, "warped," and uneven lattice fringes within the structure of amorphous zircon.

Several observations can be drawn from TEM studies that support and clarify the X-ray diffraction results. First, the amorphization process is clearly heterogeneous. Even at low doses there are isolated regions that appear to be amorphous in high-resolution images. The rotated crystalline islands observed by TEM in highly damaged zircon also suggests the presence of considerable strain or shearing due to the volume expansion of the amorphous material. Diffuse X-ray scattering also suggested the presence of shear waves in the crystalline lattice (Ríos and Salje 1999).

Short-range order

A variety of spectroscopic techniques have been used to study radiation damage accumulation in zircon. Depending on the technique, one may obtain information on changes in the nearest neighbor coordination geometries, the connectivity between coordination polyhedra over several coordination spheres, or the oxidation state of actinide elements (e.g., U and Pu). There is no single technique that provides all three types of information. In this section we review the spectroscopic studies of damage accumulation in zircon using X-ray absorption spectroscopy and nuclear magnetic resonance. However, the most detailed studies have used infrared and Raman spectroscopies to great advantage, and these results are summarized in the chapter by Nasdala et al. (this volume).

X-ray absorption spectroscopy. Extend X-ray absorption fine structure (EXAFS) spectroscopy is a sensitive probe of the local coordination and bonding geometry at the nearest-neighbor level; thus, EXAFS is very useful for characterizing the fully-damaged state of zircon (Barinsky and Kulikova 1977, Nakai et al. 1987, Greegor et al. 1990). Farges and Calas (1991) and Farges (1994) completed the first detailed EXAFS study of radiation damaged natural zircon. With increasing α-decay events dose, the mean <Zr-O> distance decreased by 0.06 Å with respect to crystalline zircon. The next-nearest-neighbor <Zr-Zr> distances are shorter in metamict zircon than in crystalline zircon (3.34 vs. 3.64 Å). For metamict zircon, Zr was in 7-fold coordination, as compared to the 8-fold coordination in crystalline zircon. Based on bond-valence theory (Brown and Shannon 1973), the relatively smaller Zr^{4+} cation is expected to be in 7-fold coordination, suggesting that as a result of metamictization, there is a "relaxation" of the ZrO_8 polyhedra to a more stable local configuration (Farges and Calas 1991). There was no evidence for radiation-induced decomposition into constituent oxides. In a later study, Farges (1994) suggested that at temperatures below 900 K the structure of naturally amorphized

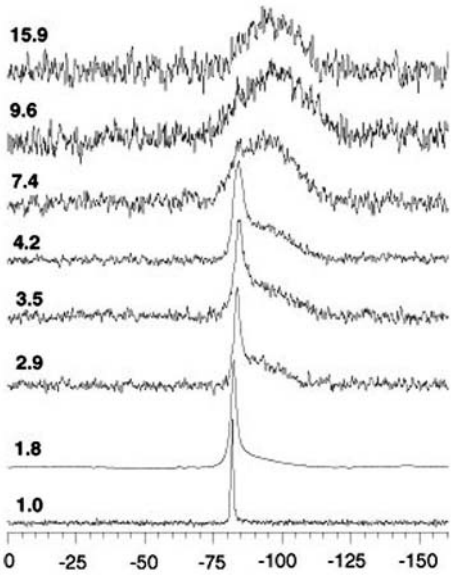

Figure 7. Series of ^{29}Si MASNMR spectra of zircon with increasing accumulated α dose (upwards). Increasing numbers indicate the dose × 10^{18} α events/g and refer to: Moroto, UG9A, Cam26, Cam25, Z5, Sand9, Ti8, and Sand4, respectively. The horizontal scale indicates chemical shift in ppm. [Used by permission of the American Institute of Physics, from Farnan and Salje (2001) *Journal of Applied Physics*, Vol. 89, Fig. 2, p. 2085.]

zircon consists of Zr- and Si-rich "nanodomains" with separate oxygen networks.

Pu-doped zircon ($Zr_{0.92}Pu_{0.08}SiO_4$) powders were synthesized with different ratios of ^{238}Pu and ^{239}Pu (Exharos 1984, Weber 1990) and studied using XAS by Begg et al. (2000). Because of the differences in half-life for the Pu isotopes (87.7 and 24,100 years, respectively) different α-decay doses were obtained for each sample. In experiments that lasted over 18 years, the ^{239}Pu-doped zircon remained highly crystalline after a dose of 1.2×10^{17} α-decays/g, while the ^{238}Pu-doped zircon was fully-metamict at a dose of 2.8×10^{19} α-decays/g. Based on X-ray diffraction analysis there was no evidence of long-range periodicity in the highly-damaged ^{238}Pu-zircon; however, the amorphous state retained the distorted, nearest-neighbor zircon structure, consisting of rotated ZrO_8 and SiO_4 tetrahedra (Begg et al. 2000), consistent with the interpretation of XAS results by Barinsky and Kulikova (1977) for fully-metamict natural zircon. Begg et al. (2000) found no evidence to Zr and Si-rich domains of different coordination numbers.

Nuclear magnetic resonance. The XAS data provide conflicting interpretations of the coordination of Zr (7 vs. 8) in the fully-damaged state. It may be reasonable to expect both types of coordination polyhedra in the aperiodic structure of the fully-damaged zircon. The retention of 8-fold coordination of Zr in the highly distorted structure suggests the possibility of some polymerization of the [SiO_4] units. Farnan (1999) used magic-angle spinning NMR to compare a natural zircon crystal that had experienced only $0.5\text{-}0.8 \times 10^{18}$ α-decays/g with one that had experienced a more significant α-decay dose (1.8×10^{18} /g). MAS-NMR is particularly sensitive to polymerization of SiO_4 tetrahedra. In the lower-dose zircon, a sharp peak was observed at a chemical shift of -81.6 ppm. This peak is characteristic of ^{29}Si in isolated SiO_4 tetrahedra. In the higher-dose sample, the ^{29}Si peak was slightly wider and an additional broad component centered at -90 ppm was identified. This slightly larger chemical shift corresponds to silicon tetrahedra sharing two bridging oxygens. In fact, the broad nature of this peak suggests that the number of shared oxygens per SiO_4 tetrahedron ranges from 0 to 4 in the higher-dose sample.

Farnan and Salje (2001) obtained a more complete picture by characterizing a suite of samples ranging in dose from 1.0×10^{18} to 15.9×10^{18} α-decays/g (Fig. 7). The NMR peak corresponding to ^{29}Si in isolated tetrahedra first broadens and shifts from -81.5 to -83.7 ppm. Farnan (1999) also observed the broadening of the ^{29}Si peak, and tentatively attributed it to contributions to the NMR signal from strain or defects in the still-crystalline regions. The peak shift may be due to increased polymerization, even in the crystalline areas. Farnan and Salje (2001) confirmed the development of a broad peak at a slightly higher chemical shift, characteristic of damaged or amorphous zircon. This amorphous peak also gradually shifted from -86 to -96 ppm with increasing dose, signifying increased polymerization. These combined changes suggest that the structures of both the crystalline and the amorphous regions are not constant but evolve continuously with increasing α-decay dose. This observation was interpreted in terms of the percolation model of Salje et al. (1999) and Trachencko et al. (2000) who noted that the structure of crystalline and amorphous zircon is different in the three percolation regimes.

Polymerization of the SiO_4 tetrahedra, as implied by the NMR data, is consistent with the earlier EXAFS results (Farges and Calas 1991) that indicated a decreased coordination of the Zr in metamict zircon. However, Farnan and Salje (2001) showed that in highly damaged or amorphous zircon there is an average of 2-3 bridging oxygens per silicon tetrahedron. These are too many bridging oxygen atoms to make up for the one removed from the Zr coordination polyhedron. In order to maintain charge balance, Farnan and Salje therefore suggested the presence of oxygen interstitials in metamict zircon.

Farnan (1999) observed that the integrated intensities of the sharp and broad peaks can be used to give a measure of the amount of Si in "amorphous" regions, assuming that the concentrations of paramagnetic defects and U^{4+} are negligible (both cause nearby silicon atoms to be undetectable). Farnan and Salje (2001) used the integrated peak intensities to determine the amorphous fraction as a function of α-decay dose. The results did not show a sigmoidal increase in the amor-

phous fraction, f_a, with dose, which agrees with the X-ray diffraction results of Ríos (2000a) and the infrared spectroscopy results of Zhang et al. (2001). At low doses, the amorphous fraction detected by NMR was higher than that expected from macroscopic volume swelling, which implies negligible swelling of amorphous domains. This is consistent with X-ray diffraction results that suggest a densification of amorphous regions below the first percolation point.

Recovery of radiation damage

The final damaged microstructure of metamict zircon depends on the kinetics of damage accumulation and the kinetics of defect recovery and/or recrystallization. These processes are highly dependent on the ambient temperature and on the irradiation conditions (e.g., dose rate, ion mass and energy, presence of impurities, etc.). In some instances, the recovery processes dominate, and crystallinity is preserved, even at relatively low temperatures. In one of the more striking mineralogical examples, monazite ($CePO_4$) remains crystalline despite extremely high α-decay doses (Meldrum et al. 1996, 1998a, 2000). In contrast, natural zircon is frequently found in a moderately- to highly-damaged state, suggesting that the kinetics of the recovery mechanisms are slower in zircon than in monazite. Recrystallization of zircon is a complex process in which several intermediate phase assemblages may form, depending on annealing conditions and the initial microstructure. Studies of the microstructural evolution on annealing of radiation-damaged zircon have been complemented by recent thermodynamic results (Ellsworth et al. 1994). This combination of microstructural and thermodynamic data can provide a more complete picture of the recrystallization mechanisms in zircon.

Recrystallization mechanisms. In general, there are two broad types of recrystallization mechanisms. Type I recrystallization is purely thermal: it occurs on time scales longer than cascade quench times and is due to defect diffusion processes. In general, Type I recovery processes dominate at longer times or at higher temperatures and become particularly important in natural specimens stored at ambient conditions for geologic periods. Type II recrystallization occurs during irradiation—it is a nearly instantaneous process that either decreases the amount of residual damage produced by each displacement event or leads to the annihilation of pre-existing irradiation-induced defects or other types of damage. Type II annealing can be divided into at least two distinct processes. Type IIa recrystallization is due to the increased mobility of interstitials and other point defects during irradiation. This "irradiation-enhanced diffusion" leads to a greater degree of point defect recombination and annihilation. Point defect annihilation is most effective at structural boundaries between amorphous and damaged, but still-crystalline, regions. Type IIb recrystallization occurs within individual displacement cascades. Disordered and highly energetic material can recrystallize epitaxially at the cascade peripheries as the displacement cascade cools to ambient temperature. As the temperature is increased, the cascade cooling time increases from picoseconds to nanoseconds or longer, increasing the effectiveness of Type IIb recrystallization. Type IIb recrystallization has not been directly observed due to the very short timescales involved, but its effects on damage accumulation have been well analyzed and modeled since its elaboration in the classic papers by Morehead and Crowder (1970a,b), and recent experimental evidence supports the importance of this process (Newcomer et al. 1996).

During irradiation, both Types I and II recrystallization processes contribute to dynamic recovery of zircon, but some mechanisms may be more dominant than others in certain temperature regimes. Type I recrystallization can be particularly important in natural samples. Its effects can be straightforwardly investigated and characterized in controlled experiments in which radiation-damaged zircon is thermally annealed in the laboratory. In contrast, Type II recrystallization processes cannot be directly investigated because of the short timescales. However, techniques in which the competing effects of damage accumulation and recrystallization can be simultaneously measured *in situ* can illuminate the effects of Type II recrystallization. With the help of computer simulations, the complex and dynamic damage and recovery processes that occur during picosecond to nanosec-

ond timescales are now better understood than ever before.

Type I recrystallization. In moderately damaged zircon that still retains a significant fraction of crystalline material, Farges (1994), Geisler et al. (2001a), and Zhang et al. (2000c) described a two-stage damage recovery process. In the first stage, X-ray diffraction measurements of air-annealed zircon showed a progressive decrease of the *a* cell parameter with increasing temperature. This effect saturated at ~600°C (Farges 1994). Geisler et al. (2001a) found that the first stage occurs below ~727°C (1000 K) and is characterized by the recovery of short-range order and point defect recombination, as measured by the shift of Raman bands to higher phonon frequencies. Zhang et al. (2000c) observed lattice recovery of partially damaged zircon at temperatures as low as 727°C. When the first stage is complete, the zircon consisted of well-crystallized regions interspersed with still-amorphous domains. The onset of the second stage occurs at higher temperatures. Above 727°C (Zhang et al. 2000c) or 893°C (Geisler et al. 2001a), the ν_3 Raman line-widths decrease and the scattering intensity increases, suggesting a decrease in the amorphous fraction caused by epitaxial recrystallization at the internal crystalline-amorphous boundaries. An initially broad and poorly defined infrared reflectivity peak at 900-1000 cm^{-1} recovered at ~727°C when annealed in an N_2 atmosphere (Zhang et al. 2000a). Above 600°C, Farges (1994) reported an increase in the intensity of the Bragg peaks and a gradual increase in the coordination of the Zr cations from seven-fold to eight-fold. This structural reorganization was completed at 900°C. Each of these observations is consistent with high-temperature epitaxial recrystallization of amorphous zircon.

Capitani et al. (2000) performed *in-situ* heating experiments in a transmission electron microscope in order to directly observe the damage recovery process. In a moderately damaged sample ($7\text{-}8 \times 10^{18}$ α-decays/g), the initial microstructure consisted of nanoscale grains of crystallographically oriented zircon embedded in an amorphous matrix. These crystalline domains increased in size at a temperature of 827°C (1100 K). This recrystallization occurred epitaxially at the boundaries of the particles. At 927°C, the pre-existing crystalline domains continued to grow but nanoscale grains of tetragonal ZrO_2 nucleated in the still-amorphous regions. At 1127°C, there were no amorphous domains or ZrO_2 remaining, and the sample consisted of a single crystal of zircon.

The somewhat different temperatures reported in these studies for the onset of epitaxial thermal recrystallization of moderately damaged zircon may be due to the different annealing environments. As noted by Pidgeon et al. (1966) and Geisler et al. (2001b), annealing under hydrothermal conditions is much faster than in an ambient, dry atmosphere. Meldrum et al. (2002a, and references therein) reported faster annealing of perovskites when annealed in air, as compared to the high-vacuum environment in the TEM. These observations are consistent with the slightly higher temperatures reported by Capitani et al. (2001) for TEM-annealed zircon as compared to the studies of Zhang et al. (2000a) and Geisler et al. (2001a). Furthermore, as reported by Biagini et al. (1997), X-ray diffraction is less sensitive to residual damage in annealed specimens than infrared spectroscopy. Therefore, the different techniques may also account for the temperature differences summarized above.

In contrast to the case of moderately damaged specimens, heavily damaged or amorphous zircon segregates into its constituent oxides at high temperatures. For example, Ellsworth et al. (1994) reported the formation of ZrO_2 only in the most damaged annealed zircon. Zhang et al. (2000a) heated a highly damaged sample (15.9×10^{18} α-decays/g) in an N_2 ambient. Above 827°C, the sample decomposed into a mixed assemblage of tetragonal ZrO_2 and amorphous SiO_2. Capitani et al. (2000) observed the formation of randomly-oriented <10 nm grains of tetragonal ZrO_2 at 927°C. Continued heating to 1127°C increased the size of the ZrO_2 nanocrystals to 30 nm. Zhang et al. (2000c) reported the formation of tetragonal ZrO_2 at 850°C. Weber (1990) observed a peak in density recovery at 1050°C in the Pu-substituted samples, which was attributed to the formation of some ZrO_2, as observed by XRD (in a nitrogen atmosphere glove-box). Begg et al. (2000) annealed Pu-substituted zircon that was fully amorphous, as determined by powder XRD. The Pu-substituted zircon decomposed into its constituent oxides at 1000°C. McLaren et al. (1994) observed the for-

mation of ZrO_2 at 900°C, in strongly zoned, chemically variable zircon annealed in dry air. In their specimens, heavily damaged optically isotropic zones alternated with less damaged anisotropic zones. Zirconia crystallites approximately 10 nm in diameter were observed to form in both the optically isotropic and anisotropic zones.

At higher temperatures, several authors have reported that the tetragonal ZrO_2 crystallites convert to the monoclinic polymorph, baddelyite. McLaren et al. (1994) observed that at 1250°C, the ZrO_2 in optically isotropic (i.e., amorphous) zones transformed to baddeleyite with a grain size of ~100 nm, but the initially anisotropic zones reverted to single-crystal zircon containing isolated baddeleyite crystallites. Zhang et al. (2000c) reported the formation of baddeleyite at 1327°C, in their heavily damaged samples. The formation of monoclinic zirconia is not reported in all investigations, so its presence may also be related to the annealing conditions and the microstructure of the specimens.

As the temperature increases, the phase-segregated oxides recrystallize to randomly-oriented polycrystalline zircon with a grain size of up to several hundred nanometers. This process is completed between 1127 and 1227°C (Zhang et al. 2000a, 2002), 1300°C (Nasdala et al. 2002a), and 1327°C (Capitani et al. 2000). Weber (1990) could not unambiguously determine the onset temperature for recrystallization of Pu-doped zircon, but found that the process was completed at 1465°C. Begg et al. (2000) reported that the Pu-substituted zircon decomposed into the component oxides at 1000°C and reverted to crystalline zircon at 1200°C. Zhang et al. (2000c) found that full recovery of the zircon structure requires temperatures in excess of 1227°C. In contrast, Pu-doped specimens that were heated rapidly to 1200°C recrystallized directly to polycrystalline zircon, without first decomposing into the constituent oxides (Begg et al. 2000).

These studies show that for slow or stepwise heating, recrystallization of heavily damaged zircon takes place in three stages:

1. Decomposition of amorphous zircon into tetragonal ZrO_2 crystallites and amorphous SiO_2. The SiO_2 is structurally distinct from conventional SiO_2 glass (e.g., Zhang et al. 2000c). This stage occurs at temperatures up to 1127°C.
2. Tetragonal-to-monoclinic phase transformation in the ZrO_2 crystallites. When reported, this stage occurs at temperatures up to 1327°C. This transition appears to depend on the time and temperature during stepwise heating experiments and is not reported in all experiments.
3. Formation of coarse-grained (several hundred nanometers), randomly oriented, polycrystalline zircon. This stage has been observed at temperatures between 1127 and 1465°C.

The energetics of radiation damage recovery reported by Ellsworth et al. (1994) can be compared with the microstructure evolution discussed above. Metamict zircon was found to have the highest enthalpy relative to crystalline zircon, followed by tetragonal zirconia + silica glass, and then baddeleyite + quartz. This is exactly the same sequence as reported in Stages 1, 2, and 3. However, the formation of monoclinic zirconia at higher temperatures than the tetragonal phase may be somewhat surprising based on the known stability fields for zirconia (monoclinic ZrO_2 transforms to the tetragonal polymorph on heating above ~1200°C). In small particles, surface energy effects can play an important role in stabilizing the various phases. Due to its lower surface energy, tetragonal zirconia is, in fact, the stable room-temperature structure for particle radii below ~5 nm, when the matrix is silica glass (Meldrum et al., in press). The thermodynamics of the phase transitions in annealed zircon are, therefore, strongly affected by the ZrO_2-matrix interface.

Finally, Zhang et al. (2000c) reported the formation of an intermediate phase during recrystallization of heavily damaged zircon at temperatures between 527 and 1127°C. This phase gave characteristic Raman peaks at 670, 798, and 1175 cm^{-1}, which cannot be attributed to SiO_2 glass, ZrO_2, or zircon. The authors speculated on the presence of a new type of Si-O-Si linkage.

Type II recrystallization. By measuring the amorphization dose as a function of temperature, *in situ* irradiation experiments permit the effects of Type II recovery to be measured directly. A frequently used technique for investigating Type II recrystallization processes in zircon has involved measuring the amorphization dose as a function of temperature *in situ* during ion beam

irradiation in a transmission electron microscope. The temperatures employed must be lower than those at which Type I recrystallization can be important on the timescale of the experiment. Such measurements have been obtained for natural or synthetic zircon irradiated with Ne^+ (Devanathan et al. 1998), Kr^+ (Weber et al. 1994, Meldrum et al. 1999b), Xe^+ (Meldrum et al. 1999b), Pb^+ (Weber et al. 1999), and Bi^+ (Weber et al. 1999; see Fig. 9 below). At low temperatures, the amorphization dose is relatively constant for all ion masses. As the temperature increases, a point is reached at which the measured amorphization dose begins to increase. At this temperature, recrystallization processes compete with damage accumulation on the timescale of the experiment. For the Kr^+ and Xe^+ irradiations, the amorphization curve appears to follow a two-step dependence on temperature. The low-temperature recovery stage was attributed to recombination and annihilation of isolated defects (Type IIa annealing); whereas, the high-temperature stage was attributed to enhanced, epitaxial recrystallization at cascade peripheries (Type IIb annealing). This behavior is not duplicated in the Pb (Meldrum, unpublished data) and Bi (Weber et al. 1999) irradiation results.

At higher temperatures, the amorphization doses increase rapidly and, at the so-called critical temperature (T_c), Type II (and/or Type I) recrystallization is so efficient that the zircon does not become electron-diffraction amorphous. The critical temperature can be estimated from the data in Figure 8 as the temperature at which the amorphization curve goes to infinity. Depending on the mass of the incident ions, the critical temperature for zircon is between 527 and 750°C and with the exception of the 600 keV Bi irradiation, T_c increases somewhat with increasing ion mass. The mass-dependent increase in T_c has been observed for many materials and is due to the structure of the damaged material (e.g., Koike et al. 1989). More massive ions produce more concentrated damaged regions; whereas, light ions produce isolated defects and smaller displacement cascades that anneal more rapidly at lower temperatures.

The critical temperature for zircon is unusually high, compared to most other minerals and ceramics (see Ewing et al. 2000). Type II recrystallization is, therefore, slower or less effective in zircon than for many related phases. Particularly striking is the difference between zircon-structure orthosilicates and orthophosphates. The critical temperatures for the orthosilicate phases are higher by several hundred degrees (Meldrum et al. 2000), with only a modest dependence on structure type. This has been attributed to the lower connectivity of the PO_4 tetrahedra, which would permit easier rotation and reorganization of these structural units. In contrast, the possible high connectivity of the SiO_4 tetrahedra in zircon imposes more severe structural constraints on the recrystallization process (Hobbs 1994).

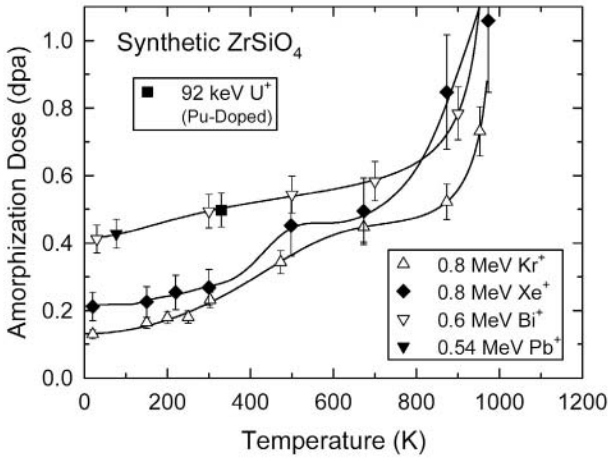

Figure 8. Temperature dependence of amorphization dose in synthetic zircons under irradiation with different ions and including the results from alpha decay in Pu-doped zircon. [Used by permission of the Materials Research Society, from Weber et al. (1999) in *Microstructural Processes in Irradiated Materials* (edited by S.J. Zinkle et al.), *Materials Research Society Symposium Proceedings*, Vol. 540, Fig. 1, p. 368.]

Meldrum et al. (1998b, 1999b) showed that nanocrystalline zirconia can precipitate during Kr^+ or Xe^+ irradiation of crystalline zircon at temperatures above ~775°C. The tetragonal zirconia occurred as

randomly oriented grains approximately 3 nm in diameter surrounded by an amorphous SiO_2 matrix. This phase decomposition occurred at lower temperatures (<675°C) in zircon that was pre-amorphized by ion irradiation. The precipitation of tetragonal zirconia was attributed to the formation of a liquid-like state in the collision cascades, followed by nucleation of ZrO_2 during the cascade-cooling phase. The ZrO_2 nucleates at higher temperatures in crystalline zircon than in pre-amorphized zircon because of competition with Type IIb recrystallization at the cascade peripheries. Another possible interpretation of the results of Meldrum et al. (1998b) is that the zirconia forms purely as a result of irradiation-enhanced cation diffusion at elevated temperatures; therefore, the formation of zirconia has less to do with the evolution of the displacement cascade. Interestingly, the zirconia nanoparticles are themselves susceptible to irradiation-induced amorphization at temperatures below 450°C (Meldrum et al. 2002b), in contrast to bulk ZrO_2, which cannot be amorphized by ion irradiation.

Recrystallization in geologic environments. Recrystallization and defect recovery are kinetic processes that are strongly dependent on time and temperature. Processes that are only apparent at high temperatures in the laboratory may be important at considerably lower temperature over geologic time. The early results were somewhat contradictory concerning the recrystallization of zircon at low temperatures over long timescales. Lumpkin and Ewing (1988) found that the calculated dose for the amorphization of natural zircon increased with the geologic age due to annealing. Using a model based on the fission-track fading, they calculated a "half life" of 400 Ma for the α-recoil damage cascades in zircon. The calculated half-life should depend on the damage rate and the recovery kinetics (specifically, temperature). While Weber et al. (1994) initially reported similar amorphization doses for ion-beam-irradiated and Sri Lanka zircon, more recent analysis (Weber et al. 1999) showed that the amorphization dose for ion-beam-amorphized natural zircon is less than that for α-decay-amorphized Sri Lanka zircon, suggesting some recovery on geologic time scales. Likewise, a comparison of unit-cell parameters (as discussed above) for lightly damaged zircon (Weber 1990) shows strong evidence of lattice relaxation along the *a*-axis in Sri Lanka zircon as compared to neutron-irradiated and Pu-doped zircon, supporting defect recovery in lightly-damaged zircon over geologic time.

Nasdala et al. (1998) found that the U-Pb isotope discordance in zircon does not always correlate with the degree of damage as estimated by the width of the ν_3 Raman peak—possibly as a result of annealing at temperatures above 227°C (Geisler et al. 2001b). Nasdala et al. (2001b) reported that zircon stored in geologically "cold" environments shows no appreciable recrystallization. However, such specimens were rare and most of the zircon specimens, including those from Sri Lanka, provided evidence in favor of recrystallization over geologic time, as determined by the narrower-than-expected ν_3 peak. Complete retention of damage was only observed at the lowest α–decay doses; whereas, at higher doses the ν_3 Raman peak-broadening increasingly deviates from the expected linear relationship (Nasdala et al. 2001, Balan et al. 2001). However, Geisler et al. (2001b) suggested that "geologic" recrystallization is only significant at high temperatures (they calculated that it would take 370 Ma to recrystallize "metamict" zircon at a temperature of 700°C). Some disagreement remains as to the interpretation of the Raman spectroscopic data and how the long-term Type I annealing affects the measured Raman bandwidth and frequency (e.g., see Geisler and Pidgeon 2002, Nasdala et al. 2002a).

Meldrum et al. (1998a, 1999a) found that the amorphization dose for natural zircon can be higher than that measured by the *in-situ* laboratory experiments. They observed that since thermal recrystallization is a diffusion-driven process, it occurs at all temperatures, but at different rates. A model was derived that accounted separately for Type I and Type II recrystallization, which allowed the ion beam irradiation data to be compared to data on natural zircon over a wide range of geologic ages (Fig. 9). The curves in Figure 9 are extrapolated from the irradiation data and represent the onset of observable damage (lower curve) and "complete" amorphization (upper curve), as measured by electron diffraction. The data points represent literature data on "crystalline" and "metamict"

zircon from a wide range of sources. The important point here is that the data sets are broadly consistent with the ion beam results (i.e., the structural state of zircon generally plots in the expected field) despite the different experimental techniques used to measure the degree of damage and the different thermal histories of the various specimens.

There are two implications inherent in Figure 9. First, the results suggest that it is possible to extract information from the ion irradiation experiments that is directly applicable to α-decay-damaged zircon, despite the enormous difference in dose rate. This was accomplished by including Type I (thermal recrystallization) in the model of damage accumulation and recovery. Second, the generally consistent results in Figure 9 imply that given enough time, zircon can recrystallize at geologically "cool" temperatures. Temperatures as low as 100-200°C seem to be sufficient to produce measurable recovery effects over extremely long time scales. This result is consistent with the observation of recovery in various suites of zircon (Nasdala et al. 2001) and with the long-term annealing of damage cascades as modeled by Lumpkin and Ewing (1988).

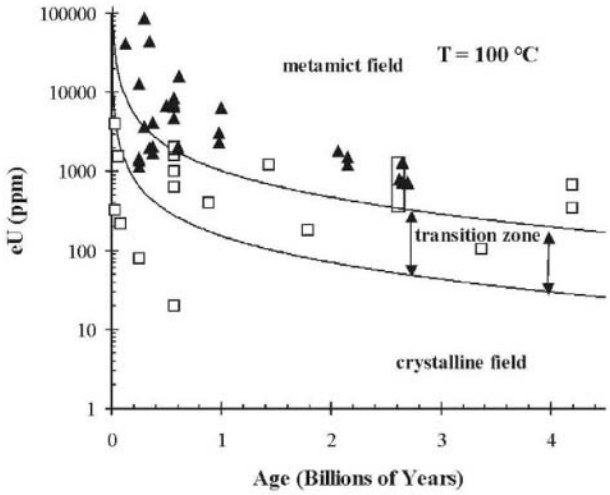

Figure 9. Crystalline-to-amorphous transition plotted as functions of equivalent uranium content and age. The lower curve represents the onset of observable damage as measured by electron diffraction, and the upper curve is for "complete" amorphization, at a temperature of 100°C. The open squares represent natural "crystalline" zircon from a variety of locations whose age and equivalent uranium content were measured or calculated. The filled triangles are for "amorphous" natural zircon from different localities. The curves delineate the crystalline-amorphous boundary fairly well, despite the different thermal histories and geologic environments of the different specimens. At higher ambient temperatures, the transitions would be shifted to higher uranium content. [Modified after Meldrum et al. (1999a).]

Recrystallization of radiation-damaged zircon is a complex, multifaceted process that involves different physical mechanisms. Purely thermal, diffusion-driven recrystallization is probably the dominant mechanism in natural zircon, even at relatively low geologic temperatures. The ultimate microstructure depends sensitively on the damage and recovery rates and on the annealing temperature. In contrast, recrystallization that occurs during ion bombardment is largely responsible for the structure of the damaged state. If this recrystallization mechanism is effective, the total atomic disorder produced per damage event will be relatively low. Physically realistic modeling of the various simultaneous damage and recovery processes in zircon present a unique and difficult challenge that will be described in more detail in the following section.

MODELS OF DAMAGE ACCUMULATION

During the past decade, there has been a major effort to model the damage accumulation process in natural, Pu-doped and ion-irradiated zircon. As previously discussed, each of these experiments provides different amounts of damaged material, from the single crystals of natural zircon to the thin damaged layers of irradiated zircon, and the irradiation experiments are completed at very different dose rates. A critical aspect of the modeling effort has been the determination of the amorphous fraction, for which the measured value is different depending on the type of analytical

technique used, as the analytical method implicitly defines the damaged volume that is considered to be amorphous. One of the most sensitive methods of measuring the amorphous fraction has been the recent use of a 7-circle diffractometer to measure the diffuse diffraction signals from single crystals of zircon (Ríos et al. 2000a). Their results provide strong evidence in support of the direct impact model of damage accumulation; however, with natural samples there is always the issue of annealing over geologic periods. Thus, in this section, we focus the review on data obtained by ion beam irradiations of zircon.

Because of the close, although not perfect, correspondence between the results from actinide-doping experiments (U, Th and Pu) and ion beam experiments (Weber et al. 1994, Weber and Ewing 2000, 2002) substantial effort has been devoted to systematic ion beam experiments combined with *in situ* TEM examination because the irradiation conditions and temperature (-260 to 1000°C) can be carefully controlled. The ion beam studies investigate the effects of temperature, ion mass and energy on the amorphization dose. These studies provide important information on the formation of collision cascades and defect annealing mechanisms (Weber et al. 1994, SX Wang et al. 1998, Weber et al. 1999 and SX Wang et al. 2001). A good summary of the different models can be found in Weber (2000). The experimental data for ion beam-irradiated zircon are designed to test and refine these models.

Temperature

The dose required for complete amorphization of zircon irradiated by 1.5 MeV Kr^+ increases with temperature in two distinct stages (Fig. 10) (Weber et al. 1994), a behavior similar to that observed in Ni_xTi_{1-x} alloys (Delage et al. 1989). The increase in amorphization dose with temperature (Fig. 10) may be due either to a decrease in the average cascade size caused by thermal relaxation or a reduction in the surviving amorphous volume as a result of thermal annealing of irradiation-induced defects. The first stage (Stage I), which occurs below 300 K, may, as an example, be associated with the intra-cascade recombination of closely-spaced defects, such as the close-pair recombination process suggested by Delage et al. (1989). As the temperature increases above 300 K, the Stage I annealing process ends (Stage I defects have recombined), and the dose for complete amorphization is constant, independent of temperature, between 300 to 473 K. Above 473 K, the amorphization dose again increases with temperature (Stage II), perhaps due to additional intra-cascade recombination of point defects or as a result of irradiation-enhanced epitaxial recrystallization (point defect annihilation at the crystalline-amorphous interface). The second stage (Fig. 10) is a common feature in irradiated

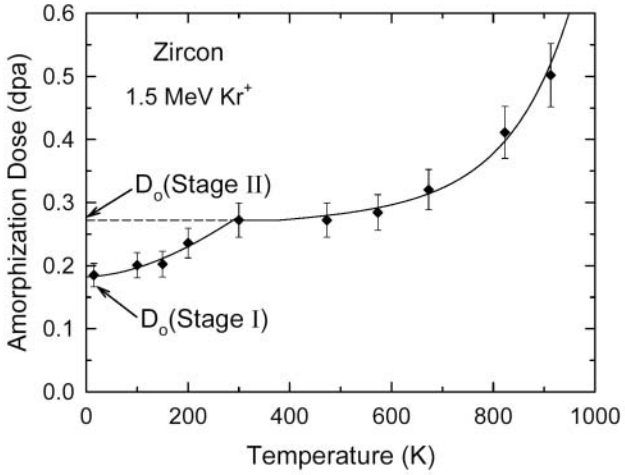

Figure 10. Temperature dependence of amorphization dose in natural zircon under irradiation with 1.5 MeV Kr^+ ions. [Based on Weber et al. (1994, 1999).]

materials, as well as zircon, and is generally ascribed to irradiation-enhanced recovery processes in amorphization models. Thermal recovery processes alone would exhibit a much sharper increase in amorphization dose with temperature (Weber 2000), and this type of behavior was illustrated in the model used to describe recent set of systematic data for orthosilicates (Meldrum et al. 1999c). Minerals can show a wide variety of behaviors, depending on their structures and compositions, and the two-stage process is not commonly observed (Ewing et al. 2000).

Regardless of the mechanism of damage recovery, the temperature dependence of amorphization dose has be described by the following expression (Weber and Wang 1993, 1994):

$$\ln(1 - D_o/D) = \ln(1/\varphi\sigma\tau) - E_a/kT, \quad (8)$$

where D is the amorphization dose at temperature, T, D_o is the extrapolated amorphization dose at 0 K associated with the damage accumulation stage, φ is the ion flux, σ is the cascade damage cross section, τ is a time constant, and E_a is the activation energy for the irradiation-assisted recovery process. A more general form of Equation (8) that has been used for a wide range of materials has been given by Weber (2000):

$$\ln[1 - (D_o/D)^{1/m}] = C - E_a/nkT, \quad (9)$$

where C is a constant dependent on damage rate and both m and n are model dependent order parameters.

Using the model described by Equation (8), an activation energy, E_a, associated with each dynamic recovery stage was determined from the data in Figure 10. The amorphization dose, D_o, associated with each dynamic recovery stage is also shown in Figure 10. For Stage I, D_o is estimated to be 0.18 dpa, and for Stage II, D_o is estimated to be 0.27 dpa. An Arrhenius plot of $\ln(1 - D_o/D)$ versus 1/kT (Weber et al. 1994) yields E_a as the slope. The activation energy determined by linear regression analysis for Stage I is 0.02±0.01 eV, and the activation energy determined for Stage II is 0.31±0.03 eV. Incorporating these parameters into Equation (8) provides an excellent fit to the data in Figure 10, as shown by the curve. Using a more complex model that assumes only thermal annealing and experimental data obtained under slightly different irradiation conditions, Meldrum et al. (1999a) obtained activation energies of 1.0 to 1.8 eV for Stage I and 3.1 to 3.6 eV for Stage II. As noted by Weber (2000), the dynamic recovery processes within each stage are probably more complex than the single activation energy process suggested by either the irradiation-assisted recovery model represented by Equation (8) or the thermal recovery model of Meldrum et al. (1999a). The actual behavior probably involves both irradiated-assisted and thermal recovery processes, but the number of parameters involved makes fitting to limited data sets challenging.

The low value of the activation energy for Stage I determined by Weber et al. (1994) suggests an irradiation-enhanced close-pair recombination process, while the higher activation energy of Meldrum et al. (1999a) suggests a thermal diffusion process. In either case, or combination thereof, these processes occur nearly instantaneously above 300 K. While these recovery processes are insufficient to prevent complete amorphization, they reduce the amount of damage that survives each cascade at temperatures above 300 K. Weber et al. (1994) noted that the activation energy determined for Stage II annealing in zircon is similar to activation energies reported in other materials for an irradiation-enhanced epitaxial recrystallization, which is a process stimulated by the irradiation-induced defects. The thermal activation energies of 3.1 to 3.6 eV determined for Stage II by Meldrum et al. (1999a) are in reasonable agreement with the activation energy, 3.6 eV, for thermal track annealing (epitaxial thermal recrystallization) in zircon (Virk 1995). As noted above, the actual behavior in zircon may be due to a more complex combination of all of these recovery processes. Nevertheless, as the temperature approaches the temperature for amorphization, T_c, the dynamic recovery rates become increasingly large, competing with the damage production rate. Above T_c, the damage recovery rates dominate and inhibit amorphization.

A general relationship for the dependence of amorphization temperature on activation energy can be derived from all these models (Weber et al. 1994, Meldrum et al. 1999a, Weber 2000) and expressed as:

$$T_c = E_a/[k \ln \Omega], \quad (10)$$

where Ω is a constant that is independent of damage rate for irradiation-assisted processes and dependent on damage rate for thermal recovery processes (Weber 2000). In Equation (8), Ω is given by $1/\varphi\sigma\tau$, which has been determined from the fit of the equation to the data in Figure 10. Using these parameters and Equation (10), the critical temperature, T_c, for zircon under these irradiation conditions is estimated to be 1101 K. In general, this is not an accurate way to determine T_c. However, Weber and Ewing (2002) have reported that T_c for synthetic zircon is 975 K for a range of ions at a given dose rate and, thus, T_c appears to be controlled mainly by thermal recovery processes. Using these results and Equation (10), Weber and Ewing (2002) predicted the dose rate dependence of T_c for plutonium-containing zircon. By extending this analysis to the lower damage rates of natural minerals, the value for T_c for zircon should have an upper limit of 460 K.

The models represented by Equations (8) and (9), as well as similar models on the temperature dependence of amorphization dose, are limited and can only be applied to data of the type shown in Figure 8. As such they do not describe the evolution of damage, but only the temperature dependence of attaining the final amorphous state. Thus, data of the type shown in Figure 10 cannot be used to confirm the mechanism of amorphization. Determining the mechanism of amorphization requires data on the evolution of the amorphous state, expressed as an amorphous fraction as a function of dose. While such models have been derived for various amorphization mechanisms (Weber et al. 1994, Meldrum et al. 1999a, Weber 2000), the mechanism of amorphization remains problematic due to a lack of data and limitations in directly measuring the amorphous fraction. Depending on the analytical technique, the "amorphous" fraction may include defect-rich crystalline domains or even isolated defects.

Based on a model of direct impact and cascade overlap, SX Wang et al. (1998, 2001) developed a different approach to describe irradiation-induced amorphization. In their model, each incident ion was assumed to create a small amorphous volume due to the rapid "quenching" of the "molten"-like displacement cascade. By analogy, the amorphization process was considered to be the result of "cascade quenching." The general features of a "quenched" cascade are similar, that is a less dense amorphous core, surrounded by halo of high defect density that grades into the crystalline matrix. Because of the presence of the crystalline matrix around the amorphous cascade core, the dominant recrystallization process is epitaxial annealing at the amorphous domain boundaries. Thus, epitaxial-recrystallization was assumed to be the recovery process during cascade "quenching."

The equation that describes the damage accumulation process is based on the damage volume of a single cascade. The formation of the individual displacement cascade with a volume, V_0, was initially assumed to remove all of the crystallinity within its boundary. The "crystallization efficiency," A, represents the volume fraction of the recrystallized shell within a single cascade, for a crystalline matrix. If there are amorphous "cores" left in the displacement cascades, the amorphous fraction will accumulate with the increasing ion dose. Because epitaxial growth relies on a crystalline interface, an increasing amorphous fraction in the material reduces the extent of recrystallization of a cascade. This process is described by the following differential equation:

, (11)

where N is the number of ions; m is the number of individual sub-cascades created by one incident ion; V_T is the total volume of the thin sample (or the damaged layer); V_c is the crystalline volume within V_T; V_0 is the volume of a sub-cascade. The recrystallized volume may develop in any direction from that surface. In this model, Wang et al. (2001) have adopted a simple description of the recrystallization process: with the last term at the right hand side of Equation (11). Integrating the equation from zero to N ions (the initial condition is that $V_c/V_T = 1$ when N = 0) and using D for ion dose, the amorphous fraction, f_a, is:

$$f_a = 1 - \frac{1}{\sqrt{A + (1-A)\cdot \exp\left(\frac{mV_0}{h}\cdot 2(1-A)\cdot D\right)}} \tag{12}$$

where h is the sample thickness (assuming h < ion range).

The amorphous fraction as a function of ion dose has been plotted for different crystallization efficiency values using Equation (12). For small A, f_a behaves as a simple exponential function. For large A, especially for A close to 1, the $f_a \sim D$ curve is sigmoidal, and the sigmoidal character of the curve becomes more obvious with increasing A. When A = 1, f_a is zero regardless of dose. Thus the different $f_a \sim D$ curve shapes previously assumed to represent different amorphization mechanisms (Gibbons 1972), i.e., from defect accumulation to multiple cascade overlap to direct impact cascade amorphization, may all be explained by the cascade "quenching" model by only varying the crystallization efficiency parameter, A. Because A represents the recrystallization efficiency, it must vary with the temperature and the properties of the target material. The recrystallization efficiency may be given by:

$$A = A_0 \cdot \exp[-E_a/(k\ T)], \tag{13}$$

where A_0 is a pre-exponential constant; E_a is the activation energy for the dynamic annealing of a cascade; k is the Boltzmann's constant; T is the sample temperature.

The pre-exponential constant, A_0, can be determined by specifying a boundary condition. According to Equation (13), A increases with increasing temperature. When the temperature reaches a certain value, A equals 1 (A approaches 1 with increasing temperature because this causes a decrease in the cascade volume due to recrystallization). At a critical temperature, T_c, the entire damaged volume is recrystallized (no further amorphization occurs when $T \bullet T_c$). Using T_c as a boundary condition, Equation (13) becomes:

$$A = \begin{cases} \exp\left[\dfrac{E_a}{k}\left(\dfrac{1}{T_c} - \dfrac{1}{T}\right)\right], & for \quad T < T_c \\ A = 1, \quad for \quad T \geq T_c \end{cases} \tag{14}$$

or

$$A \mid \begin{cases} \left\{1 - \dfrac{T_c - T}{T_m - T}\right\}^b, & for \quad T \{ T_c \\ A \mid 1, \quad for \quad T \varnothing T_c \end{cases} \tag{15}$$

where b is a sub-cascade shape-parameter that has a value between 2 to 3, depending on cascade shape (b = 2 for a cylinder, b = 3 for a sphere, 2 < b < 3 for an ellipsoid); T_m is the melting temperature of the target material; T_c is the critical temperature of the sample above which full recrystalli-

dose have been derived and simplified as:

$$D_c = \frac{D_0}{1 + \exp\left[\frac{E_a}{k}\left(\frac{1}{T_c} - \frac{1}{T}\right)\right]} \tag{16}$$

or

$$D_c = \frac{D_0 (T_c / T_m)^3}{\left(\frac{T_c - T}{T_m - T}\right)^3}, \tag{17}$$

where D_0 is the amorphization dose extrapolated to T = 0 K. D_0 incorporates all the temperature independent terms (h, m, V_0 and Δ_c). This model also provides an excellent fit to the temperature dependence of amorphization dose in zircon under 1.5 MeV Kr^+ irradiation (SX Wang et al. 2001).

Ion mass and energy

Irradiations of single crystals of zircon have been completed at room temperature with 1.5 MeV Xe^+, 0.7 MeV Kr^+, 1.5 MeV Kr^+, 1.5 MeV Ar^+, 0.8 MeV Ne^+, 0.54 MeV Pb^+ 0.6 MeV Bi^+ ions to investigate the effects of damage energy density (eV/nm/ion) on the amorphization dose (Weber et al. 1994, 1999). Complete amorphization occurred for all ions and energies. The effect of the damage energy density on the amorphization dose is shown in Figure 11. Also shown is the amorphization dose (2.3 dpa) for a 2 MeV He^+ implant in zircon, as well as the amorphization dose (0.59 dpa) corresponding to f_a = 95% in polycrystalline Pu-doped zircon (this dose calculation includes only the 92 keV U^+ recoil-nucleus contribution). These results show that the amorphization dose under the high dose rates (~10^{-4} to 10^{-3} dpa/s) for heavy-ion irradiations is nearly identical to that of Pu-doped zircon (3×10^{-9} dpa/s), which suggests that the amorphization process is independent of the damage source and dose rate. The minimum in amorphization dose for the 1.5 MeV Ar^+ irradiation, as compared to the heavier ions, may reflect the greater survivability of point defects from intra-cascade recombination due to the smaller cascade size created by the lower average recoil energy. In the case of Ne^+ and He^+ irradiation, the damage consists of a larger fraction of isolated displacements (point defects) and small well-separated displacement sub-cascades. Consequently, significant recovery of the isolated point defects (e.g., close pairs) will occur during irradiation, and substantial cascade overlap, particularly for the He^+ irradiations, is required to achieve the critical defect density for amorphization. These results have shown that the kinetics of amorphization are qualitatively different for light and heavy ions.

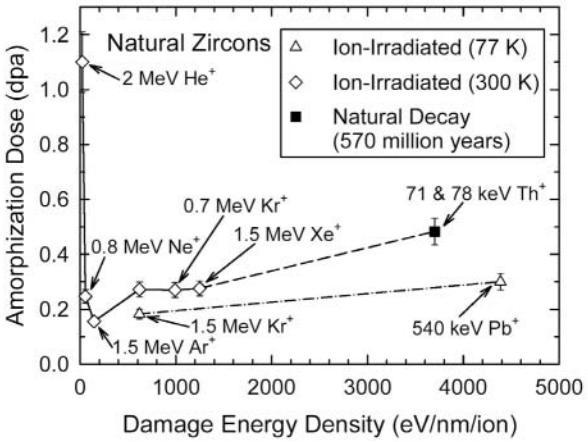

Figure 11. Dependence of amorphization dose on damage energy density in natural zircons under different irradiation conditions. [Modified from Weber et al. (1999).]

Recently, Weber et al. (1999) have summarized all of the ion beam irradiation results for zircon. The general fea-

tures of the damage process are clear: The amorphization dose for zircon exhibits two distinct stages with increasing temperature (Fig. 10). The transition temperature between stages for natural zircon occurs at a much lower temperature (300 K) than for synthetic zircon (500 K), perhaps due to the presence of impurities in the natural zircon. The amorphization dose also increases with damage energy density, as determined by varying the mass and energy of the ions. This is behavior may seem to be inconsistent with the direct impact model, but also may reflect the effect of changes in the cascade size and geometry on relaxation and recrystallization processes. At present, no single model captures the behavior of zircon from the three types of radiation experiments, and different analytical techniques sample different volumes of "damaged" material. The three models that we have presented (Weber et al. 1994, Meldrum et al. 1999a, SX Wang et al. 2001) are certainly over simplifications of the damage accumulation process; however, they do give the reader a good sense of the types of processes that occur during the damage process. There are at present a variety of models, some representing combinations of processes (Weber 2000), but no single analytical technique provides the required resolution over all dose ranges to distinguish among these models. The critically missing information has been the description of cascade formation and relaxation processes and the interactions between the cascades as they overlap. This has led to the recent spate of simulation studies described in the next section.

COMPUTER SIMULATION OF DEFECT FORMATION AND RADIATION DAMAGE

Atomistic computer simulations have been used to understand atomic-level processes related to the radiation damage process during cascade formation. Theoretical methods, such as *ab initi*o calculations and molecular dynamics (MD) simulations, are used to study the behavior of intrinsic, or native, defects (e.g., interstitials and vacancies) and extrinsic defects associated with impurities, and to determine the minimum energies required to permanently displace atoms due to the transfer of kinetic energy. With the advent of large-scale computing, MD simulations are also used to determine the distribution and nature of intrinsic defects, extended defect structures, and solid-state transformations resulting from the collision cascade produced by energetic ions, such as the α-particle and recoil nucleus produced in an α-decay event. At present, three computer simulation methods have been used to study intrinsic defects and radiation damage processes. One is based on well-established static-lattice energy minimization methods (Catlow and Mackrodt 1982, Agullo-Lopez et al. 1988), and another is based on MD methods (Agullo-Lopez et al. 1988, Eckstein 1991). Both employ empirical interatomic potentials to describe the interactions between all atoms (e.g., Zr-O, Zr-Zr, Si-O; Si-Si, and Zr-Si). The third method, which is applicable only to defect production from ion-solid interactions, is the binary collision approximation, BCA, (Eckstein 1991, Robinson 1994) that employs a universal scattering potential to describe the scattering physics between atoms. The BCA is a higher energy approximation, in which the trajectories of energetic particles are simulated by a series of two-body collisions. Static-lattice methods are essentially "zero Kelvin" calculations, with no representation of thermal effects. In contrast, MD simulations include the kinetic energy explicitly by solving, in an iterative numerical procedure, Newton's equations of motion for an ensemble of particles. The main limitation of the MD technique is the narrow range of time-scales (picoseconds to nanoseconds) that can be simulated.

Computer simulation of radiation damage processes in metals and semiconductors is a mature area of research (Guinan and Kinney 1981, Robinson 1994, Gao and Bacon 1995, Gao and Weber 2002, Nord et al. 2002), where the results provide important atomic-level insights into the radiation damage process and interpretation of experimental data. In contrast, computational studies of defects and radiation damage processes in zircon are a rather new effort (Crocombette and Ghaleb 1998b, Meis and Gale 1998, Williford et al. 1998). The essential concern in the application of these techniques is that the interatomic potentials must not only accurately describe the crystal structure, but also the elastic constants, defect formation and migration energies, and the hard-sphere scatter-

ing physics of energetic particles at short interaction distances.

Intrinsic and extrinsic defect energies

The formation energies of native defects and impurities in zircon are important to: (1) identifying the lowest energy configurations for interstitial and vacancy defects, (2) determining the probability for stable anti-site defects, and (3) identifying the stable configurations for incorporation of impurities, such as U, Th and Pu, and the decay-products, such as helium. In addition, the migration energies of the intrinsic defects determine the nature of the damage recovery processes and self-diffusion mechanisms that occur as a function of time and temperature.

Static, energy minimization methods, using classical potentials based on either rigid ion or shell models, have been used to determine the formation energies of vacancy and Frenkel defects in zircon (Meis and Gale 1998, Williford et al. 1999, Akhtar and Waseem 2001, Park et al. 2001). The standard method for determining the formation energy of a vacancy is to calculate the difference in bulk potential energy, with and without the defect, correcting appropriately for the chemical potential of the affected species. Despite their differences, it is useful that classical interatomic potentials yield formation energies for vacancies on the order of 80, 105, and 24 eV for Zr, Si, and O, respectively. These are rather high, but do not consider the defect reactions necessary to form a vacancy by actual Schottky or Frenkel mechanisms, which maintain charge neutrality and stoichiometry. Based on different interatomic potentials, the formation energies for intrinsic Frenkel defects (interstitial-vacancy pairs) on the Zr and O sublattices have been calculated to be 9.4 and 8.2 eV by Meis and Gale (1998), 15.6 and 6.3 eV by Akhtar and Waseem (2001), and 31.7 and 9.0 eV by Park et al. (2001), respectively. A more accurate determination of the defect formation energies may be obtained by *ab initio* methods. These methods have been applied to determine the structural properties of the low-pressure and high-pressure phases of zircon with high accuracy (Crocombette and Ghaleb 1998a), and similar methods have been applied to determine the defect formation energies (Crocombette 1999). The *ab initio* calculations yield formation energies for Zr, Si, and O vacancies of 5.9, 5.8 and 5.6 eV, respectively, and for Zr, Si, and O interstitials of 18.0, 17.0, and 1.7 eV, respectively (Crocombette 1999). The formation energies for intrinsic Frenkel defects, determined by *ab initio* calculations, are 24.0, 22.9, and 7.3 eV for Zr, Si, and O, respectively. Using classical potentials, the formation energy for the Si intrinsic Frenkel defect is estimated to be 13.9 eV (Akhtar and Waseem 2001) or 24.3 eV (Park et al. 2001). There are considerable differences between the *ab initio* and classical potential results, particularly for the cations, that are not sufficiently understood. However, all the results indicate high formation energies, which suggests that it should be difficult to form intrinsic defects in zircon.

Based on rigid ion classical potentials, the migration energies for Zr and O vacancies along different paths have been calculated (Williford et al. 1999). Both Zr and O vacancies migrate three-dimensionally with activation energies of 1.27±0.11 and 1.08±0.09 eV, respectively. These low vacancy migration energies, suggest radiation-induced vacancies should migrate and anneal in the crystalline structure at intermediate temperatures at laboratory time scales and at ambient temperatures over geologic time scales. Migration energies have not been calculated for interstitial defects. The activation energy for thermal diffusion is the sum of the formation and migration energies for the defect responsible for diffusion. The activation energy (8.4 eV) for Hf diffusion has been experimentally determined by Cherniak et al. (1997), which should be similar to that of Zr because of their similar size and charge. Likewise, the activation energy for O diffusion (4.7 eV) has been experimentally determined by Watson and Cherniak (1997). If thermal self-diffusion occurs by intrinsic vacancy migration, as is usually assumed, and if the calculated vacancy migration energies are reasonably accurate, then the formation energies for intrinsic vacancies are much lower than the calculated Frenkel defect energies. Either the calculations have large errors or another intrinsic vacancy formation process, such as the Schottky defect, may occur. However, both *ab initio* (Crocombette 1999) and classical potential (Akhtar and Waseem 2001) calculations indicate higher

formation energies of 34.1 and 8.52 eV, respectively, for intrinsic Schottky defects.

The formation energy (9.4 eV) for the extrinsic defect formed by the substitution of U^{4+} for Zr^{4+} has been determined using classical potentials (Meis and Gale 1998). Because of the interest in using zircon to immobilize plutonium, the formation energy of Pu^{4+} substitution for Zr^{4+} was determined to be 8.3±0.2 eV using classical potentials (Meis and Gale 1998, Williford et al. 2000), while that of Pu^{3+} substitution for Zr^{4+} is 37.75 eV (Williford et al. 2000). The lower energy for substitution of Pu^{4+} relative to U^{4+} may be due to the slightly smaller ionic radius of Pu as compared to U. By taking into account the defect and lattice formation energies, the actual energy required for the substitution of U^{4+} for Zr^{4+} is 0.28 eV per U atom (Akhtar and Waseem 2001), while that for the substitution of Pu^{4+} for Zr^{4+} is 0.26 eV per Pu atom (Williford et al. 2000). In the case of Pu^{3+} substitution on the Zr^{4+} site, as might be the case for preparation under reducing conditions, the lowest energy defect configuration (1.02 eV per Pu atom) is for a defect cluster consisting of two Pu^{3+} substitutions on near-neighbor Zr^{4+} sites and a neighboring charge-compensating oxygen vacancy (Williford et al. 2000, Muller and Weber 2001).

Using transition state theory (Henderson 1972), the activation energies for self-diffusion in zircon of U^{4+} and Pu^{4+} in the presence of intrinsic vacancies are 5.9 and 5.6 eV along the [021] direction, respectively; and 9.3 eV for both U^{4+} and Pu^{4+} along the [111] direction (Meis and Gale 1998). The calculated activation energy for U diffusion is slightly lower than the average experimental value (7.5 eV) determined for U self-diffusion (Cherniak et al. 1997). This suggests formation energies for intrinsic vacancies of 1.5 to 2.0 eV, much lower than those calculated.

Threshold displacement energies

One of the fundamental parameters affecting radiation damage in a material is the threshold displacement energy, E_d, which is the minimum kinetic energy necessary to displace an atom from its normal site. The parameter E_d is essential for quantifying an irradiation dose in terms of the number of displaced atoms in the irradiated material, which allows quantitative comparisons of α-decay event damage with neutron or ion-beam irradiation damage. Static energy minimization methods using classical potentials were first employed to determine the threshold displacement energies in zircon (Williford et al. 1998). Similar calculations have been performed more recently (Meis, personal communication). The results are summarized in Table 1. While the Zr and O displacement energies are similar, there is a significant difference in the Si displacement energies that result from differences in interatomic potentials. The threshold displacement energies of Williford et al. (1998) have been used in comparisons of radiation damage in zircon due to α-decay and ion irradiations (Weber et al. 1999).

Two studies (Park et al. 2001, Crocombette and Ghaleb 2001) have used classical potential based MD simulations to determine threshold displacement energies (Table 1). The results of the MD study by Park et al. (2001) showed that threshold displacement events occur at energies ranging from 23 to 200 eV. In nearly all cases, the threshold displacement events produce multiple displacements (multiple Frenkel pairs, antisite defects and replacements). The production of a single Frenkel pair is rare. The threshold displacement energies determined by Park et al. (2001) are significantly less than those calculated by Crocombette and Ghaleb (2001).

With the exception of the early results by Williford et al. (1998), the more recent static and MD results in Table 1 are consistent in that oxygen has a much lower displacement energy than Zr or Si, which exhibit comparable displacement energies (within 10 eV). While there are few experi-

Table 1. Calculated threshold displacement energies in zircon.

Method	*Zr (eV)*	*Si (eV)*	*O (eV)*	*Reference*
energy minimization	80	20	45	Williford et al. 1998
energy minimization	76	85	38	Meis, personal communication
molecular dynamics	90	98	32	Crocombette & Ghaleb 2001
molecular dynamics	60	48	23	Park et al. 2001

mental results, the displacement energies for Zr in Table 1 are in reasonable agreement with the values (41 to 97 eV) estimated for Zr in zircon from experiment (Devanathan et al. 1998).

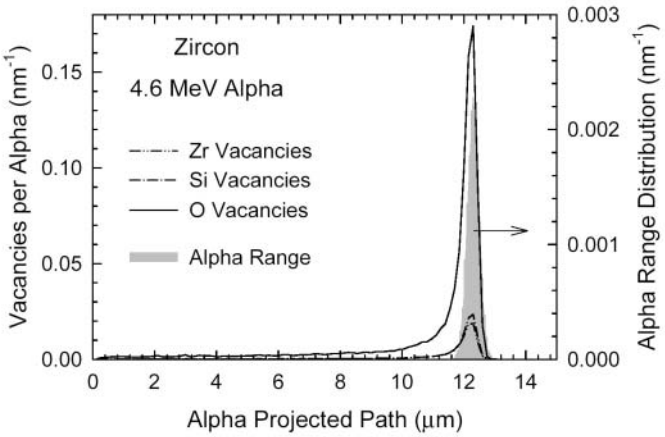

Figure 12. Calculated number of vacancies produced along the path of 4.6 MeV alpha particles in zircon, along with the distribution of alpha particle ranges, using the BCA code SRIM.

Collision cascades

Energetic α-particles in an α-decay event dissipate most of their energy by ionization processes over a range of 16 to 22 μm, but undergo enough elastic collisions along their path to produce several hundred isolated atomic displacements. The largest number of displacements occurs near the end of the alpha-particle range. The partitioning of the energy loss by alpha-particles between ionization and elastic collisions, the range of the alpha particles, and the distribution of displaced atoms, if the threshold displacement energies are known, can be determined by computational approaches based on the binary collision approximation (BCA). The more massive but lower energy alpha-recoil particle accounts for most of the total number of displacements produced by alpha decay in zircon. The alpha-recoil loses nearly all of its energy in elastic collisions over a very short range (30 to 40 nm), producing a highly localized collision cascade of 1000 to 2000 displacements. The density of energy deposited into the crystal structure by an alpha-recoil cascade is high (up to 1 eV/atom) and occurs over a very short time ($<10^{-12}$ s). The spatial extent of the alpha-recoil cascade can be calculated reasonably well by BCA codes, but the binary collision approximation is generally not as quantitative for determining the number of displacements or nature of the damage on such a localized cascade. The binary collision approximation also does not account for any simultaneous recombination events that may occur. Molecular dynamic simulations provide the only means of calculating the primary damage state in such cascades. While such simulations can be performed, the results are sensitive to interatomic potentials, and current methodologies limit the range of energies that can be simulated.

Given the threshold displacement energies, the production of displacements in these polyatomic materials by ballistic processes can be determined by computational approaches based on the binary collision approximation (BCA). These computational approaches generally involve using codes, such as TRIM (Ziegler et al. 1985, Ziegler 2002) and MARLOWE (Robinson 1994, Oak Ridge National Laboratory 2002), in which the elastic atomic scattering is described by a universal screened scattering potential. The universal screened scattering potential developed by Ziegler, Biersack and Littmark (1985), the ZBL potential, is most commonly used because it provides a reasonably accurate description of the nuclear stopping power and energy dissipated by elastic atomic scattering collisions, which has been demonstrated by consistent agreement with experimental measurements of scattering cross sections and energetic particle ranges in solids. The TRIM (Transport and Range of Ions in Matter) code assumes an aperiodic solid and uses a Monte Carlo method to determine the scattering angle and energy transfer that results from each binary elastic collision. TRIM is now part of a package of programs in SRIM (Stopping and Range of Ions in Matter) (Ziegler 2002). MARLOWE is a BCA code that does take into account atomic-scale periodicity. The binary collision approximation, however, is a high-energy approximation that is most appropriate for high-energy collisions and for light ions, e.g., α-particles. Using the threshold displacement energies

from Park et al. (2001), calculations with TRIM of the atomic displacements produced by the 4.6 MeV α-particle from the decay of ^{235}U are shown in Figure 12 as a function of projected range. The average range of the α-particle is 12.1±0.3 μm, and a total of about 178 displaced atoms, mostly oxygen, are produced by each α-particle, primarily near the end of the range.

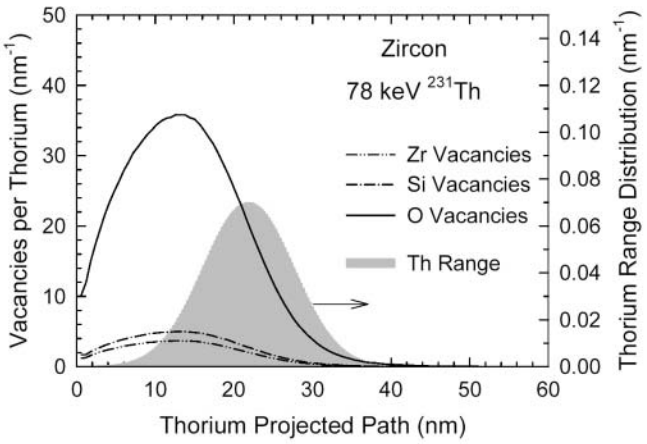

Figure 13. Calculated number of vacancies produced along the path of 78 keV ^{231}Th recoils in zircon, along with the distribution of Th ranges, using the BCA code SRIM.

At low energies the trajectories of recoils are not easily described by discrete collisions, such as in an α-recoil cascade, and the BCA is less useful because it fails to account for the simultaneous recombination of Frenkel pairs, as well as amorphization processes that may be associated with high-energy deposition. However, the spatial extent of the cascade and range of the α-recoil are well described by the BCA. Using the same threshold displacement energies as above, TRIM calculations for 78 keV ^{231}Th recoils released in α-decay of ^{235}U in zircon are shown in Figure 13, as a function of projected range. The average range for 78 keV ^{231}Th α-recoils is 21.7±5.7 nm, and a total of 932 atoms are displaced by elastic collisions, mostly oxygens. Similar results are obtained using MARLOWE, which incorporates the structure of zircon, and a typical α-recoil cascade is illustrated in Figure 14. The ^{231}Th recoil shown in Figure 14 has a range of 24 nm, and the cascade exhibits the branching typical of sub-cascade development. Because MARLOWE, and other BCA codes, do not account for defect recombination or collective displacements associated with direct impact amorphization, the region of high defect density along part of the U recoil track may occur as an amorphous domain in an actual material.

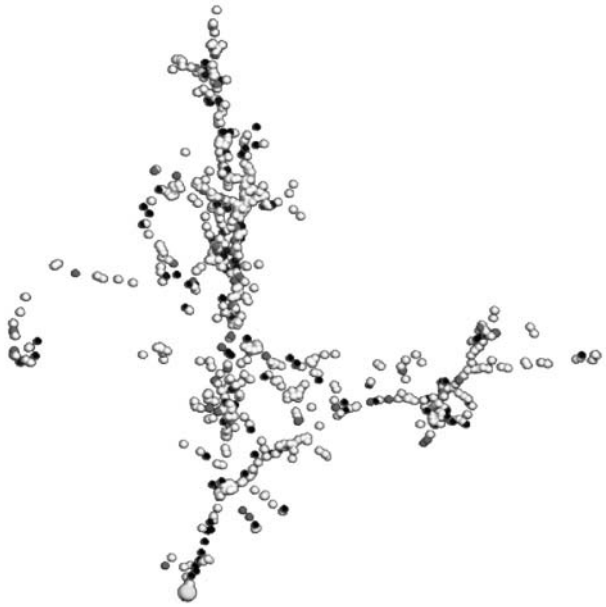

Figure 14. Calculated spatial distribution of vacancies produced by a typical 78 keV ^{231}Th recoil in zircon using the BCA code MARLOWE.

While MD simulations provide the only means of eventually calculating the nature of the primary damage state from energetic cascades in zircon, the total volume necessary to contain the α-recoil cascade in Figure 14 is 1.56×10^4 nm^3, containing 1.44 million atoms. Such large arrays of atoms with their complex interactions cannot be handled by current MD calculations. Thus, MD simulations of realistic α-recoil cascades are not presently feasible, and MD simu-

lations of α-particle cascades may remain beyond the computational capability of MD methods for some time to come. As a result, the BCA calculations provide the most realistic simulation of α-particle damage, and those on α-recoils provide a good representation of the spatial extent of the cascade and the branching that is expected due to sub-cascade formation. The BCA codes provide a means of semi-quantitatively comparing the results from ion-beam irradiation of zircon by different masses and energies and with the results of self-radiation due to α-decay. In many materials, the essential physics of damage production can be obtained from less energetic cascades, and the standard approach is to investigate cascade damage production as a function of recoil energy. The recoils can be incorporated U or self-ions, such as Zr, Si, or O.

Because of the small time (picoseconds) and distance scales (tens of nanometers) associated with damage production, MD simulations are ideally suited for the study of primary damage processes and understanding the atomic-level dynamics of the structural response to a recoil event. Studies of cascades in oxides, such as zircon, by MD simulation have been limited by the computational cost associated with the long range of the Coulomb interaction and the lack of reliable interatomic potentials. For MD simulations of displacement cascades, the interatomic potentials need to describe the structure, elastic constants, and defect energies, as well as correctly describe the physics of classical atomic scattering, within the repulsive component of the potential, that is associated with the energetic elastic collision processes. Classical atomic scattering and nuclear stopping are well described by the ZBL universal scattering potential developed by Ziegler et al. (1985). As a result, experienced researchers have long employed the ZBL potential to describe the short-range interactions in MD simulations of collision cascades in metals, semiconductors, and oxides. Under such conditions, the ZBL potential is smoothly fitted to the potential for medium-range and long-range interactions. Alternatively, some researchers have used *ab initio* quantum mechanical calculations to determine the repulsive nature of the interatomic potential, but even under these conditions, the ZBL potential is often used as a benchmark for validating the potential. It is important to note that while the BCA codes take into consideration both electronic and nuclear interactions, the MD approach generally only considers the nuclear (i.e., elastic scattering) interactions.

Due to computational constraints, most MD simulations of zircon have been of low-energy displacement cascades (Crocombette and Ghaleb 1998b, 1999, 2001; Devanathan et al. 2002, Trachenko et al. 2001, 2002). Crocombette and Ghaleb (1998b, 1999, 2001) used a Born-Mayer-Huggins potential fit to the ZBL potential for atomic distances less than 0.1 nm. Similarly, Devanathan et al. (2002) used the rigid ion potential of Park et al. (2001) with energy partitioned into long-range (Coulombic) interactions, short-range (Buckingham-type potential) interactions, and close-pair (ZBL potential) interactions. Trachenko et al. (2001) used a Coulombic model with Buckingham-type and three-body potentials, but no modification was made to account for the hard-sphere collisions at short interaction distances. Trachenko et al. (2002) did use a short-range repulsive potential correction to the Buckingham-type potential; however, the repulsive potential differs significantly from the ZBL potential and predicts significantly larger scattering cross sections for some atom pairs. This affects the interactions and ranges of the primary and secondary recoils, thus affecting the distribution in energy deposition and spatial extent of the cascade. The differences in the potentials, and perhaps, in the simulation methodologies, have led to significant differences in the results reported by Trachenko et al. (2001, 2002) and others (Crocombette and Ghaleb 1998b, 1999, 2001; Devanathan et al. 2002).

Crocombette and Ghaleb (1998b) investigated low energy displacement cascades initiated by self-ions with energies from 0.5 to 2.0 keV. They also investigated the cascade produced by 4 and 5 keV U recoils in pure zircon (containing only the one U substituted for Zr) and in which 4 and 12% of the Zr atoms are replaced by U (Crocombette and Ghaleb 1999, 2001). As expected, they found a linear increase in crystal volume with increasing U. Both self-ions (Zr, Si, and O) and the U recoils produced displaced atoms, with over half recovering to their original sites within less than a picosecond. They did not observe the collective movement of the silicon tetrahedra, as has been

observed in glasses (Delaye and Ghaleb 1997), and they reported that no displaced Si atom had the same oxygen neighbors before and after the collision. The low-energy U-cascades result in the creation of a cylindrical amorphous region along the path of the U-recoil, which has a range of about 4 to 5 nm. The amount of disorder decreased from the core to the outer shell of the track. The structure of the amorphous core is similar to that of the bulk amorphous volume created by a MD simulation of a melt-quenched zircon. The number of oxygen displacements is a factor of 5 to 20 higher than either the Zr or Si displacements, which is generally consistent with the more recent calculations of threshold displacement energies (Table 1). Surprisingly, no isolated point defects are observed. Many Zr atoms exhibited a decrease in coordination number from eight to seven or six in the cascade core, which is consistent with some experimental observations (Farges and Calas 1991, Farges 1994, Hess et al. 1998). At the same time, they observed some Si atoms are coordinated by five O atoms, which they attribute to a possible non-physical aberration of the empirical potential due to the lack of three-body terms. While the SiO_4 tetrahedra in crystalline zircon are isolated, they exhibit some polymerization in the core of the cascade. However, some connectivity between SiO_4 tetrahedra is expected due to the random displacement and relaxation of individual atoms. There are experimental NMR (Farnan and Salje 2001) and infrared absorption (Zhang and Salje 2001) evidence for some SiO_4 polymerization in natural zircons, but synthetic zircons irradiated at room temperature do not exhibit significant polymerization (Begg et al. 2000). The polymerization observed in these MD studies (Crocombette and Ghaleb 1999, 2001) and other similar studies (Devanathan et al. 2002, Trachenko et al. 2002) might be an artifact of using empirical potentials for Si-Si and Si-O interactions derived for quartz.

Low-energy displacement cascades that are caused by 0.25 to 1.0 keV Zr recoils were investigated by Devanathan et al. (2002). The displacement cascade is linear (cylindrical) along the ion track, similar to previous observations (Crocombette and Ghaleb 2001), due to inefficient energy transfer between the sublattices associated with the differences in threshold displacement energies (Table 1) and atomic masses. Figure 15 illustrates the evolution of displaced atoms (only vacancies) produced by a 1 keV Zr cascade. An atom is considered displaced if it moved out of its Wigner-Seitz cell (i.e., a space-filling polyhedral cell centered at each atom in the original crystal structure). Devanathan et al. (2002) preferred this criterion to the criteria employed by others (Crocombette and Ghaleb 2001, Trachenko et al. 2001) that are based on the distance moved by an atom, because in the latter case the number of displacements varies with the displacement cutoff distance chosen and the choice of this distance is arbitrary. The total number of atoms displaced by a 1 keV Zr-recoil is large (110 atoms after 10 ps), and as in the case of Crocombette and Ghaleb (2001), the number of O displacements is significantly larger than the number of either Zr or Si displacements. The primary damage state produced by low-energy

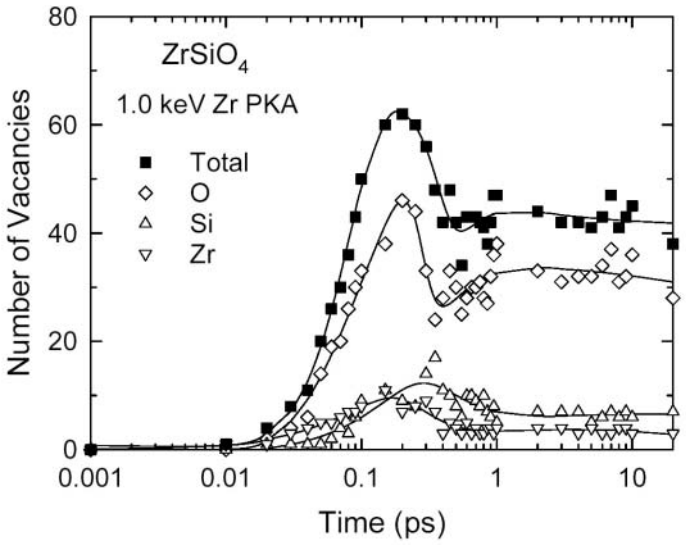

Figure 15. The total number of vacancies and number of vacancies produced on each sublattice by a 1 keV Zr recoil cascade in zircon as a function of time from the generation of the Zr recoil.

cascades consisted of O replacements produced primarily by a ring-like sequence of replacement events on the O sublattice, similar to that observed for O threshold displacement processes (Park et al. 2001), Si interstitials interconnected by O interstitials, vacancy clusters, and anti-site defects. The fraction of Si atoms with one or more bridging O neighbors increased with increasing Zr-recoil energy. While the melt-quenched state in this study exhibited a degree of SiO_4 polymerization, similar to the melt-quenched state of Crocombette and Ghaleb (2001), the number of bridging O atoms connected to other Si atoms showed a distribution from zero to four that peak at one, which is different than the distribution of Crocombette and Ghaleb (2001) that ranged from zero to five and was a maximum at two and three bridging oxygen atoms per silicon. Similarly, in the study of Devanathan et al. (2002), the melt quench state did not exhibit 5-fold coordinated Si atoms. This supports the conclusion of Crocombette and Ghaleb (2001) that this configuration may be an artifact of their potential.

The evolution of damage from 1 keV Zr-cascades were studied by Trachenko et al. (2001) using MD simulations. Similar to the results of Crocombette and Ghaleb (1998b, 1999, 2001) and Devanathan et al. (2002), they found that 1 keV Zr cascades produce more O displacements than Zr or Si displacements at 300 K, with the number of O displacements being 4 and 10 times greater than the number Si and Zr displacements, respectively. Because there are four times as many O atoms as Si atoms in zircon, this implies that the O and Si threshold displacement energies must be similar and that the Zr displacement energy is somewhat larger. This is consistent with the threshold displacement energies in Table 1. They also investigated the effects of overlapping cascades on damage production and found that the number of displacements produced by each cascade increases with each subsequent cascade. After several cascades overlapped, the number of Si and O displacements become comparable; however, the number of Zr-displacements remains about a factor of three less than either the number of Si or O displacements. They also reported polymerization of SiO_4 tetrahedra and the formation of both 5-fold and 6-fold coordinated Si in the cascades.

Trachenko et al. (2002) also studied 30 and 70 keV Zr-recoils in zircon using simulation cells containing 192,000 and 375,000 atoms, respectively. They did not observe any subcascades or branching that might be expected in such energetic cascades; instead, they found a highly polymerized sphere of SiO_n surrounding the core of the cascade. This is not too surprising for the empirical potential used, since it produces a very dense collision cascade (relative to BCA estimates) in which the O and Si displacements outnumber the Zr displacements by nearly factors of two and three, respectively. Thus, in the core of the cascade, there should be a slight excess of vacancies that is surrounded by a halo of damage containing an excess of Si and O interstitials.

UNRESOLVED RESEARCH ISSUES

Because of the importance of radiation effects on zircon in geological and materials science applications, there has been a recent, substantial effort to understand the processes and effects of α-decay event damage in zircon and related phases. Indeed, over 100 of the papers cited in this summary have been published since 1990. Even with this impressive effort, a number of important issues remain unresolved.

1. What is the "amorphous" fraction? As has been shown in the summary of the simulations of the effects of a single α-decay event, an α-recoil cascade consists of a series of different damage domains—a less-dense core surrounded by a high density of interstitial defects that grades into highly strained crystalline domains. The α-particle leaves a string of isolated defects along its trajectory with most of the ballistic interactions occurring at the end of its path. A fundamental issue is the definition of the nature of a "damaged" domain. While an isolated point defect is not usually considered to form an amorphous domain, at what point is a cluster of defects considered an "amorphous" domain? Depending on the analytical technique used to measure the "amorphous" fraction, the proportion of crystalline to amorphous volume varies, as each technique probes, with varying efficiencies, different "amorphous" volumes. The ability to distinguish among the different

amorphization mechanisms is directly dependent on our ability to determine the relationship between the amorphous fraction, f_a, and dose. However, we have made progress. We can say that the damage accumulation process is heterogeneous, that is it occurs with the formation of individual cascades and that the amorphous volume increases as the number of cascades increases. Our present analytical techniques, however, do not provide much experimental insight into what happens in individual cascades or when cascades overlap, and the present level of simulations of cascade interactions do not reach the relevant spatial and temporal scales.

2. What is the structure of amorphous zircon? Although a variety of analytical techniques have been used to study the structure of highly-damaged, "amorphous" zircon, contradictions remain. Some studies have cited evidence for Zr-rich and Si-rich nano-domains in highly damaged zircon, but for most samples this is not evident. There are differences in the estimates of the degree of increased polymerization of the [SiO_4] tetrahedral monomers. There are differences in the estimates of the coordination number of Zr (7 vs. 8) and Si (3 to 5) in damaged zircon. Indeed, there is, at present, no unique description of the fully-damaged state of zircon. Perhaps, it is unreasonable to expect a completely consistent picture to evolve from the present sample set. Clearly, natural zircon experiences different degrees of annealing with different thermal histories. The microstructure that evolves during annealing depends on the initial damage-state. For the ion beam irradiation experiments, the type of irradiation, e.g., mass and energy, and the dose rate also affect the structure. There might be more progress made if research focused on studies of carefully prepared bulk samples of amorphous material, for example by sol-gel or rapid quenching techniques, and comparison to amorphous structures produced in simulations by "quenching." The experience gained from studying these aperiodic samples could then be applied to partially- or highly-damaged zircon. Similarly, using advanced analytical techniques currently being applied to characterize the structure of nanoscale films, the structure of the thick amorphous layers (0.5 to 1.0 μm) formed during ion-beam irradiation could be characterized on single crystals of synthetic zircon.

3. What are the effects of variations in ion mass, ion energy and temperature on cascade formation? Although we will always struggle with the definition and determination of the amorphous fraction, systematic irradiations of synthetic zircon crystals with different ion energies and masses over a wide temperature range can provide data that will allow us to distinguish between different damage mechanisms and damage accumulation models. These systematic studies will necessarily resolve the wide variations in even simple calculations of the number of atomic displacements per α-decay event, which presently vary from 800 to 4,000. The experimental studies would benefit greatly by similarly systematic simulations of cascade formation over relevant energy, length and time scales.

4. To what extent does zircon anneal at low temperatures over geologic time? There is compelling evidence that the radiation damage in natural zircon can and does anneal at essentially ambient conditions. However, we have very limited data on the activation energies of the different annealing mechanisms, e.g., point defects vs. cascade recrystallization. At present, we cannot use the extent of damage annealing to reconstruct the thermal history of a natural zircon. However, given the variety of damage effects, point defects, recoil cascades and fission tracks, it may be possible to constrain the thermal history of a well-characterized zircon based on its damage microstructure.

5. What are the damage recovery processes? For moderately damaged zircon, the two stages (defect recovery in the crystalline structure, followed by epitaxial recrystallization at higher temperatures) are well described. However, the process that dominates depends on the initial damage state. The presence of isolated defects will affect the energetics of the recrystallization process. There continue to be disagreements on the relative efficiencies of point defect recovery versus recrystallization of the cascade as a function of temperature. The activation energies for the different recrystallization mechanisms are similarly problematic. Again, the contradictions in experimental results are most likely the result of using natural zircon samples that have different levels of damage and different initial microstructures. Experimental studies of damage recovery processes in

ion-beam irradiated single crystals, for which the thermal history is well controlled, and computer simulations of defect migration and recrystallization processes can provide a fundamental understanding of damage recovery processes in zircon that can be used to model recovery processes from different damage states over geologic time.

ACKNOWLEDGMENTS

All of the authors of this chapter have benefited from sustained funding by the Office of Basic Energy Sciences of the U.S. Department of Energy. This funding has enabled two decades of collaboration between university investigators, first at the University of New Mexico and now at the University of Michigan, and the colleagues at Pacific Northwest National Laboratory. During this period we have had numerous collaborators who appear as co-authors on the cited publications. These collaborations are too numerous to enumerate, but we want to emphasize that it was only through these collaborative efforts that we were able to contribute to the fundamental understanding of radiation damage effects in zircon that are summarized in this chapter. Parts of this chapter were presented by RCE in 2002 in his Presidential Address to the Mineralogical Society of America. RCE notes with gratitude the encouragement and guidance of Professor Adolf Pabst during the earliest stages of this research nearly 30 years ago. We thank John Hanchar, Lutz Nasdala, Chris Palenik, and Susana Ríos for their careful and thoughtful reviews of this chapter.

REFERENCES

Agullo-Lopez F, Catlow CRA, Townsend PD (1988) Point defects in materials. Chapter 11 In Computer Modelling Techniques. Academic Press, London, p 341-372

Akhtar MJ, Waseem S (2001) Atomistic simulation studies of zircon. Chem Phys 274:109-120

Babsail L, Hamelin N, Townsend PD (1991) Helium-ion implanted wave-guides in zircon. Nucl Instr Meth Phys Res B59/60:1219-1222

Balan E, Neuville DR, Trocellier P, Fritsch E, Muller JP, Calas G (2001) Metamictization and chemical durability of detrital zircon. Am Mineral 86:1025-1033

Barinsky RL, Kulikova IM (1977) Metamict transformation in some niobates and zircons according to X-ray absorption spectra. Phys Chem Mineral 1:325-333

Begg BD, Hess NJ, Weber WJ, Conradson SD, Scheiger MJ, Ewing RC (2000) XAS and XRD study of annealed ^{238}Pu- and ^{239}Pu-substituted zircons ($Zr_{0.92}Pu_{0.08}SiO_4$). J Nucl Mater 278:121-224

Biagini R, Memmi I, Olmi F (1997) Radiation damage in zircons. N Jahrb Mineral Monat 6:257-270

Brinkman JA (1954) On the nature of radiation damage in metals. J Appl Phys 25:961-970

Brown ID, Shannon RD (1973) Empirical bond strength-bond length curves for oxides. Acta Crystallogr A29:266-282

Burakov BE, Hanchar JM, Zamoryanskaya MV, Garbuzov VM, Zirlin VA (2002) Synthesis and investigation of Pu-doped single crystal zircon, $(Zr,Pu)SiO_4$. Radiochim Acta 90:95-97

Burakov BE, Hanchar JM, Zamoryanskaya MV, Anderson EB, Garbuzov VM, Kitsay AA, Krivovichev SV (in press) Investigation of single crystal zircon, $(Zr,Pu)SiO_4$, doped with ^{238}Pu. Radiochim Acta

Bursill LA, McLaren AC (1966) Transmission electron microscope study of natural radiation damage in zircon ($ZrSiO_4$). Phys Stat Solidi 13:331-343

Bursill LA, Braunshausen G (1990) Heavy-ion irradiation tracks in zircon. Phil Mag A62:395-420

Capitani GC, Leroux H, Doukhan JC, Ríos S, Zhang M, Salje EKH (2000) A TEM investigation of natural metamict zircons: structure and recovery of amorphous domains. Phys Chem Mineral 27:545-556

Cartz L, Fournelle R (1979) Metamict zircon formed by heavy ion bombardment. Radiation Effects 41:211-217

Catlow CRA, Mackrodt WC (eds) (1982) Computer Simulation of Solids. Lecture Notes in Physics, Vol. 166. Springer, Berlin

Chakoumakos BC, Murakami T, Lumpkin GR, Ewing RC (1987) Alpha-decay induced fracturing in zircon: The transition from the crystalline to the metamict state. Science 236:1556-1559

Chakoumakos BC, Oliver WC, Lumpkin GR, Ewing RC (1991) Hardness and elastic modulus of zircon as a function of heavy-particle irradiation dose: I. *In situ* α-decay event damage. Rad Effects Defects Solids 118: 393-403

Chen J, Lian J, Wang, LM, Ewing RC, Wang RG, Pan W (2002) X-ray photoelectron spectroscopy study of disordering in $Gd_2(Ti_{1-x}Zr_x)_2O_7$ pyrochlores. Phys Rev Lett 88:105901-1 – 105901-4

Cherniak DJ, Hanchar JM, Watson EB (1997) Diffusion of tetravalent cations in zircon. Contrib Mineral Petrol 127: 383-390.

Crawford JH (1965) Radiation damage in solids: A survey. Ceram Bull 44:963-970
Crawford JH, Wittels MC (1956) A review of investigations of radiation effects in covalent and ionic crystals. *In* Proceedings of International Conference on Peaceful Uses of Atomic Energy, vol 7, United Nations, New York, p 654-665
Crocombette J-P (1999) Theoretical study of point defects in crystalline zircon. Phys Chem Mineral 27:138-143
Crocombette J-P, Ghaleb D (1998a) Modeling the structure of zircon ($ZrSiO_4$): empirical potentials, *ab initi*o electron structure. J Nucl Mater 257: 282-286
Crocombette J-P, Ghaleb D (1998b) Molecular dynamics simulation of displacement cascades in zircon ($ZrSiO_4$). *In* Scientific Basis for Nuclear Waste Management XXI. McKinley IG, McCombie C (eds) Mater Res Soc Symp Proc, vol 506, Warrendale, Pennsylvania, p 101-108
Crocombette J-P, Ghaleb D (1999) Molecular dynamics simulation of recoil nucleus displacement cascade in zircon. *In* Microstructural Processes in Irradiated Materials. Zinkle SJ, Lucas GE, Ewing RC, Williams JS (eds) Mater Res Soc Symp Proc, vol 540, Warrendale, Pennsylvania, p 343-348
Crocombette J-P, Ghaleb D (2001) Molecular dynamics modeling of irradiation damage in pure and uranium-doped zircon. J Nucl Mater 295:167-178
Delage J, Popoola O, Villain JP, Moine P (1989) Temperature-dependence of amorphization and precipitation processes in Ni^+ implanted and N^+ implanted Ni_xTi_{1-x} alloys. Mater Sci Engr A115:133-138
Delaye J-M, Ghaleb D (1997) Molecular dynamics simulations of low-energy atomic displacement cascades in a simplified nuclear glass. J Nucl Mater 244:22-28
Devanathan R, Weber WJ, Boatner LA (1998) Response of zircon to electron and Ne^+ irradiation. *In* Phase Transformations and Systems Driven Far from Equilibrium. Atzmon M, Bellon P, Trivedi R (eds) Mater Res Soc Symp Proc, vol 481, Warrendale, Pennsylvania, p 419-424
Devanathan R, Weber WJ, Corrales LR (2002) Atomistic simulation of displacement cascades in zircon. *In* Scientific Basis for Nuclear Waste Management XXV. McGrail BP, Cragnolino GA (eds) Mater Res Soc Symp Proc, vol 713, Warrendale, Pennsylvania, JJ11.36.
Eckstein W (1991) Computer Simulation of Ion-Solid Interactions. Springer-Verlag, Berlin
Ellsworth S, Navrotsky A, Ewing RC (1994) Energetics of radiation damage in natural zircon ($ZrSiO_4$). Phys Chem Mineral 21:140-149
Ewing RC (1994) The metamict state: 1993 – The centennial. Nucl Instru Method Phys Res B91:22-29
Ewing RC, Haaker RF, Lutze W (1982) Leachability of zircon as a function of alpha dose. *In* Scientific Basis for Radioactive Waste Management V. Lutze W (ed) Elsevier, Amsterdam, p 389-397
Ewing RC, Lutze W, Weber WJ (1995) Zircon: A host-phase for the disposal of weapons plutonium. J Mater Res 10: 243-246
Ewing RC, Meldrum A, Wang LM, Wang SX (2000) Radiation-induced amorphization. *In* Transformation Processes in Minerals. Redfern SAT and Carpenter MA (eds) Rev Mineral Geochem 39:319-361
Exarhos GJ (1984) Induced swelling in radiation damaged $ZrSiO_4$. Nucl Instr Method Phys Res B1: 538-541
Farnan I (1999) Si-29 NMR characterization of the crystalline-amorphous transition in $ZrSiO_4$. Phase Transitions 69:47-60
Farnan I, Salje EKH (2001) The degree and nature of radiation damage in zircon observed by ^{29}Si nuclear magnetic resonance. J Appl Phys 89:2084-2090
Farges F (1994) The structure of metamict zircon: A temperature-dependent EXAFS study. Phys Chem Minerals 20:504-514
Farges F, Calas G (1991) Structural analysis of radiation damage in zircon and thorite: An X-ray absorption spectroscopic study. Am Mineral 76:60-73
Fortner JA, Badyal Y, Price DCL, Hanchar JM, Weber WJ (1999) Structural analysis of a completely amorphous ^{238}Pu-doped zircon by neutron diffraction. *In:* Mater Res Soc Symp Proc, vol. 540, Zinkle SJ, Lucas GE, Ewing RC, Williams JS (eds) Warrendale, Pennsylvania, p 349-353
Gao F, Bacon DJ (1995) Molecular dynamics study of displacement cascades in Ni_3Al: I. General features and defect production efficiency. Phil Mag A71: 43-64
Gao F, Weber WJ (2002) Cascade overlap and amorphization in 3C-SiC: Defect accumulation, topological features, and disordering. Phys Rev B66:024106-11
Geisler T, Pidgeon RT (2002) Raman scattering from metamict zircon: comments on "Metamictisation of natural zircon: accumulation versus thermal annealing of radioactivity-induced damage. Contrib Mineral Petrol 143:750-755
Geisler T, Pidgeon RT, van Broswijk W, Pleysier R (2001a) Kinetics of thermal recovery and recrystallization of partially metamict zircon: a Raman spectroscopic study. Eur J Mineral 13:1163-1176.
Geisler T, Ulonska M, Schleicher H, Pidgeon RT, van Bronswijk W (2001b) Leaching and differential recrystallization of metamict zircon under experimental hydrothermal conditions. Contrib Mineral Petrol 141:53-65
Gibbons JF (1972) Ion implantation in semiconductors—Part II: Damage production and annealing. Proc IEEE

60:1062-1096
Greegor RB, Lytle FW, Ewing RC (1990) X-ray absorption spectroscopic investigation of Zr in metamict and annealed zircon. Ann Meeting Mater Res Soc, abstr, pA24
Guinan MW, Kinney JH (1981) Molecular dynamic calculations of energetic displacement cascades. J Nucl Mater 103 & 104:1319-1323
Hayashi M, Shinno I, Taguchi S, Sugihara S (1990) ESR signals of zircon irradiated with thermal neutrons and γ-rays. J Mineral Petrol Econ Geol 85:27-33
Headley TJ, Ewing RC, Haaker RF (1981) The structure of the metamict state. Nature 293:449-450
Headley TJ, Arnold GW, Northrup CJM (1982a) Dose-dependence of Pb-ion implantation damage in zirconolite, hollandite and zircon. *In* Scientific Basis for Radioactive Waste Management V, Lutze W (ed) Elsevier Science Publishing, New York, p 379-388
Headley TJ, Ewing RC, Haaker RF (1982b) High-resolution study of the metamict state in zircon. *In* 39th Ann Proc Electron Micros Soc Am, Bailey GW (ed) San Francisco Press, San Francisco, p 112-113
Helean KB, Lutze W, Ewing RC (1999) Dissolution studies of inert materials. *In:* Environmental Issues and Waste Management Technologies in the Ceramic and Nuclear Industries IV. Marra JC and Chandler GT (eds) Am Ceram Soc Ceram Trans 93:297-304
Henderson B (1972) Defects in Crystalline Solids. Edward Arnold, London
Hess NJ, Weber WJ, Conradson SD (1998) X-ray absorption fine structure of aged, Pu-doped glass and ceramic waste forms. J Nucl Mater 254:175-184
Hobbs LW (1994) Topology and geometry in the irradiation-induced amorphization of insulators. Nucl Instru Meth Phys Res B91:30-42
Holland HD, Gottfried D. (1955) The effect of nuclear radiation on the structure of zircon. Acta Crystallogr 8:291-300
Hurley PM, Fairbairn HW (1952) Alpha-radiation damage in zircon. J Appl Phys 23:1408
Hurley PM, Fairbairn HW (1953) Radiation damage in zircon: A possible age method. Geol Soc Am Bull 64:659-674
Jonckheere R, Gögen K (2001) A Monte-Carlo calculation of the size distribution of latent alpha-recoil tracks. Nucl Instru Method Phys Res B183:347-357
Karioris FG, Gowda KA, Cartz L (1981) Heavy ion bombardment of monoclinic $ThSiO_4$, ThO_2 and monazite. Rad Effects Lett 58:1-3
Karioris, FG, Appaji Gowda K, Cartz L, Labbe JC (1982) Damage cross-sections of heavy ions in crystal structures. J Nucl Mater 108/109:748-750
Koike J, Okamoto PR, Rehn LE (1989) The dose, temperature, and projectile-mass dependence for irradiation-induced amorphization of CuTi. J Mater Res 4:1143-1150
Lee JKW, Tromp J (1995) Self-induced fracture generation in zircon. J Geophys Res 100:71,753-17,770
Lian J, Wang LM, Wang SX, Chen J, Boatner LA, Ewing RC (2001) Nanoscale manipulation of pyrochlore: new nanocomposite ionic conductors. Phys Rev Lett 87:145901-1 – 145901-4
Lian J, Ríos S, Boatner LA, Wang LM, Ewing RC (in press) Microstructural evolution and nanocrystal formation of Pb^+-implanted ZrSiO4 single crystals. J. Appl. Phys.
Lumpkin GR (2001) Alpha-decay damage and aqueous durability of actinide host phases in natural systems. J Nucl Mater 289:136-166
Lumpkin GR, Ewing RC (1988) Alpha-decay damage in minerals of the pyrochlore group. Phys Chem Minerals 16:2-20
McLaren AC, FitzGerald JD, Williams JS (1994) The microstructure of zircon and its influence on the age determination from Pb/U isotopic ratios measured by ion microprobe. Geochim Cosmochim Acta 58:993-1005
Meis C, Gale JD (1998) Computational study of tetravalent uranium and plutonium lattice diffusion in zircon. Mater Sci Engin B 57:52-61
Meldrum A, Wang LM, Ewing RC (1996) Ion beam-induced amorphization of monazite. Nucl Instru Method Phys Res B116:220-224
Meldrum A, Boatner LA, Weber WJ, Ewing RC (1998a) Radiation damage in zircon and monazite. Geochim Cosmochim Acta 62:2509-2520
Meldrum A, Zinkle SJ, Boatner LA, Ewing RC (1998b) A transient liquid-like state in the displacement cascades of zircon, hafnon, and thorite. Nature 395:56-58
Meldrum A, Zinkle SJ, Boatner LA, Wang SX, Wang LM, Ewing RC (1999a) Effects of dose rate and temperature on the crystalline-to-metamict transformation in the ABO_4 orthosilicates. Can Mineral 37:207-221
Meldrum A, Zinkle SJ, Boatner LA, Ewing RC (1999b) Heavy-ion irradiation effects in the ABO_4 orthosilicates: decomposition, amorphization, and recrystallization. Phys Rev B59:3981-3992
Meldrum A, Boatner LA, Ewing RC (2000) A comparison of radiation effects in crystalline ABO_4-type phosphates and silicates. Mineral Mag 64:183-192
Meldrum A, Boatner LA, Weber WJ, Ewing RC (2002a) Amorphization and recrystallization of the ABO_3 oxides.

J Nucl Mater 300:242-254
Meldrum A, Boatner LA, Ewing RC (2002b) Nanocrystalline zirconia can be amorphized by ion irradiation. Phys Rev Lett 88:025503-1 – 025503-4
Meldrum A, Boatner LA, Ewing RC (in press) Size effects in the irradiation-induced crystalline-to-amorphous transformation. Nucl Instru Method Phys Res
Miller ML, Ewing RC (1992) Image simulation of partially amorphous materials. Ultramicroscopy 48: 203-237
Morehead FF Jr, Crowder BL (1970a) A model for the formation of amorphous silicon by ion bombardment. Radiation Effects 6:27-32
Morehead FF, Crowder BL, Title RS (1970b) Formation of amorphous silicon by ion-bombardment as a function of ion, temperature, and dose. J Appl Phys 43:1112-1972
Muller I, Weber WJ (2001) Plutonium in crystalline ceramics and glasses. MRS Bulletin 26:698-706
Murakami T, Chakoumakos BC, Ewing RC (1986) X-ray powder diffraction analysis of alpha-event radiation damage in zircon ($ZrSiO_4$). *In* Advances in Ceramics: Nuclear Waste Management II. Clark DE, White WB, Machiels J (eds) Am Ceram Soc, Columbus, Ohio, p 745-753
Murakami T, Chakoumakos BC, Ewing RC, Lumpkin GR, Weber WJ (1991) Alpha-decay event damage in zircon. Am Mineral 76:1510-1532
Nakai I, Akimoto J, Imafuku M, Miyawaki R, Sugitani Y, Koto K (1987) Characterization of the amorphous state in metamict silicates and niobates by EXAFS and XANES analyses. Phys Chem Minerals 15:113-124
Nasdala L, Pidgeon RT, Wolf D, Irmer G (1998) Metamictization and U-Pb isotopic discordance in single zircons: a combined Raman microprobe and SHRIMP ion probe study. Mineral Petrol 62:1-27
Nasdala L, Wenzel M, Vavra G, Irmer G, Wenzel T, Kober B (2001) Metamictization of natural zircon: accumulation versus thermal annealing of radioactivity-induced damage. Contrib Mineral Petrol 141:125-144
Nasdala L, Imer G, Jonckheere R (2002a) Radiation damage ages: Practical concept or impractical vision? Reply to two comments on "Metamictisation of natural zircon: Accumulation versus thermal annealing of radioactivity-induced damage", erratum, and further discussion. Contrib Mineral Petrol 143:758-765
Nasdala L, Lengauer CL, Hanchar JM, Kronz A, Wirth R, Blanc P, Kennedy AK, Seydoux-Guillaume A-M (2002b) Annealing radiation damage and the recovery of cathodoluminescence. Chemical Geology 191:121-140
Newcomer PP, Barbour JC, Wang LM, Venturini EL, Kwak JF, Ewing RC, Miller ML, Morosin B (1996) Temperature dependent microstructural modification in ion irradiated Tl-type high temperature superconductors. Physica C: Supeconductivity 267:243-253
Nord J, Nordlund K, Keinonen J (2002) Amorphization mechanism and defect structures in ion-beam amorphized Si, Ge, and GaAs. Phys Rev B65:165329-1 – 165329-6
Oak Ridge National Laboratory (2002) http://www.ssd.ornl.gov/Programs/MARLOWE/Marlowe.htm
Oliver WC, McCallum JC, Chakoumakos BC, Boatner LA (1994) Hardness and elastic modulus of zircon as a function of heavy-particle irradiation dose: II. Pb-ion implantation damage. Rad Effects Defects Solids 132:131-141
Özkan H (1976) Effect of nuclear radiation on the elastic moduli of zircon. J Appl Phys 47:4772-4779
Pabst A (1952) The metamict state. Am Mineral 37:137-157
Palenik CS, Ewing RC, Nasdala L (in press) Radiation damage in a zoned zircon crystal. Am Mineral
Park B, Weber WJ, Corrales LR (2001) Molecular dynamics simulation study of threshold displacements and defect formation in zircon. Phys Rev B64:174108-1 – 174108-16
Pellas P (1965) Étude sur la recristallisation thermique des zircons métamictes. Mémoires du Muséum National D'Histoire Naturelle Serie C, Sciences de la Terre XII:227-253
Petit JC, Dran JC, Gianantonio DM (1987) Effects of ion implantation on the dissolution of minerals Part II: selective dissolution. Bull Minéral 110:25-42
Pidgeon RT, O'Neil JR, Silver LT (1966) Uranium and lead isotopic stability in metamict zircon under experimental hydrothermal conditions. Science 154:1538-1540
Raychaudhuri AK, Peech JM, Pohl RO (1980) Phonon scattering in glasses and highly disordered crystals. *In* Proc Third Intl Conf Phonon Scattering in Solids. Maris H (ed) Plenum Press, New York, p 1-3
Ríos S, Salje EKH (1999) Diffuse X-ray scattering from weakly metamict zircon. J Phys: Condensed Matter 11:8947-8956
Ríos S, Salje EKH, Zhang M, Ewing RC (2000a) Amorphization in zircon: evidence for direct impact damage. J Phys: Condensed Matter 12:2401-2412
Ríos S, Malcherek T, Salje EKH, Domenaghetti C (2000b) Localized defects in radiation-damaged zircon. Acta Crystallogr B56:947-952
Robinson MT (1994) Basic physics of radiation damage production. J Nucl Mater 216:1-28
Sahama TG (1981) Growth structure in Ceylon zircon. Bull Minéral 104:89-94
Salje EKH, Chrosch J, Ewing RC (1999) Is "metamictization" of zircon a phase transition? Am Mineral 84:1107-

1116
Slater JC (1951) The effects of radiation on materials. J Appl Phys 22:237-256
Speer JA (1982) Zircon. Rev Mineral 5:67-112
v Stackelberg M, Rottenbach E (1940) Dichte und struktur des zircons, III & IV. Z Kristallogr 97:173-182; 207-208
Tole MP (1985) The kinetics of dissolution of zircon ($ZrSiO_4$). Geochim Cosmochim Acta 49:453-458
Trachenko KO, Dove MT, Salje EKH (2000) Modelling the percolation-type transition in radiation damage. J Appl Phys 87:7702-7707
Trachenko KO, Dove MT, Salje EKH (2001) Atomistic modeling of radiation damage in zircon. J Phys: Condensed Matter 13:1947-1959
Trachenko KO, Dove MT, Salje EKH (2002) Structural changes in zircon under α-decay irradiation. Phys Rev B 65:180102
Trachenko KO, Dove MT, Salje EKH (2003) Large swelling and percolation in irradiated zircon. J Phys: Condens Matter 15:L1-L7
Vance ER (1975) α-Recoil damage in zircon. Rad Effects 24:1-6
Vance ER, Anderson BW (1972) Study of metamict Ceylon zircons. Mineral Mag 38:605-613
Virk HS (1995) Single activation-energy model of radiation-damage in solid-state nuclear track detectors. Rad Effects Defects Solids 133:87-95
Wang LM (1998) Application of advanced electron microscopy techniques to the studies of radiation effects in ceramic materials. Nucl Instr Meth Phys Res B141:312-325
Wang LM, Ewing RC (1992a) Ion beam induced amorphization of complex ceramic materials-minerals. Mater Res Soc Bull 17(5):38-44
Wang LM, Ewing RC (1992b) Detailed *in situ* study of ion beam-induced amorphization of zircon. Nucl Instru Method Phys Res B65:324-329
Wang LM, Eby RK, Janeczek J, Ewing RC (1991) *In situ* TEM study of ion-beam-induced amorphization of crystalline natural silicates. Nucl Instr Method Phys Res B59:395-400
Wang LM, Ewing RC, Weber WJ, Eby RK (1993) Temperature dependence of amorphization dose for ion beam irradiated zircon and olivine. *In* Mater Res Soc Symp Proc. vol 279, Nastasi M, Harriott LR, Herbots N, Averback RS (eds) Warrendale, Pennsylvania, p 451-456
Wang SX, Wang LM, Ewing RC (1998) A model for irradiation-induced amorphization. *In* Mater Res Soc Symp Proc vol 504, Barbour JC, Roorda S, Ila D, Tsujioka M (eds) Warrendale, Pennsylvania, p 165-170
Wang SX, Wang LM, Ewing RC (2001) Irradiation induced-amorphization: the effects of temperature, ion species, dose rate, and materials. Phys Rev B63:41051-41058
Watson EB, Cherniak DJ (1997) Oxygen diffusion in zircon. Earth Planet Sci Lett 148:527-544
Weber WJ (1990) Radiation-induced defects and amorphization in zircon. J Mater Res 5:2687-2697
Weber WJ (1991) Self-radiation damage and recovery in Pu-doped zircon. Rad Effects Defects Solids 115:341-349
Weber WJ (1993) Alpha-decay-induced amorphization in complex silicate structures. J Am Ceram Soc 76:1729-1738
Weber WJ (2000) Models and mechanisms of irradiation-induced amorphization in ceramics. Nucl Instr Method Phys Res B 166-167:98-106
Weber WJ, Ewing RC (2000) Plutonium immobilization and radiation effects. Science 289:2051-2052
Weber WJ, Ewing RC (2002) Radiation effects in crystalline oxide host phases for the immobilization of actinides. *In* Scientific Basis for Nuclear Waste Management XXV. McGrail BP, Cragnolino GA (eds) Mater Res Soc Symp Proc vol 713, Warrendale, Pennsylvania, p 443-454
Weber WJ, Wang LM (1993) Irradiation induced amorphization of $Ca_2La_8(SiO_4)_6O_2$ single crystals. *In* Mater Res Soc Symp Proc vol. 279, Nastasi M, Harriott LR, Herbots N, Averback RS (eds) Warrendale, Pennsylvania, p 523-528
Weber WJ, Wang LM (1994) Effect of temperature and recoil-energy spectra on irradiation-induced amorphization in $Ca_2La_8(SiO_4)_6O_2$. Nucl Instr Method Phys Res B 91:63-66
Weber WJ, Ewing RC, Wang LM (1994) The radiation-induced crystalline-to-amorphous transition in zircon. J Mater Res 9:688-698
Weber WJ, Ewing RC, Meldrum A (1997) The kinetics of alpha-decay-induced amorphization in zircon and apatite containing weapons-grade plutonium or other actinides. J Nucl Mater 250:147-155
Weber WJ, Ewing RC, Catlow CRA, de la Rubia TD, Hobbs LW, Kinoshita C, Matzke Hj, Motta AT, Nastasi M, Salje EKH, Vance ER, Zinkle SJ (1998) Radiation effects in crystalline ceramics for the immobilization of high-level nuclear waste and plutonium. J Mater Res 13:1434-1484
Weber WJ, Devanathan R, Meldrum A, Boatner LA, Ewing RC, Wang LM (1999) The effect of temperature and recoil spectra on amorphization in zircon. *In* Microstructural Processes in Irradiated Materials. Zinkle SJ, Lucas GE, Ewing RC, Williams JS (eds) Mater Res Soc Symp Proc, vol 540, Warrendale, Pennsylvania, p 367-372
Williford RE, Devanathan R, Weber WJ (1998) Computer simulation of displacement threshold energies for several

ceramic materials. Nucl Instr Method Phys Res B141: 98-103
Williford RE, Weber WJ, Devanathan R, Cormack AN (1999) Native vacancy migrations in zircon. J Nucl Mater 273:164-170
Williford RE, Begg BD, Weber WJ, Hess NJ (2000) Computer simulation of Pu^{3+} and Pu^{4+} substitutions in zircon. J Nucl Mater 278:207-211
Yada K, Takayoshi T, Sunagawa I (1981) Application of lattice imagery to radiation damage investigation in natural zircon. Phys Chem Minerals 7:47-52
Yada K, Takayoshi T, Sunagawa I (1987) Radiation induced lattice defects in natural zircon ($ZrSiO_4$) observed at atomic resolution. Phys Chem Minerals 14:197-204
Zhang M, Salje EKH, Ewing RC, Farnan I, Ríos S, Schlüter, Leggo P (2000a) α-decay damage and recrystallization in zircon: Evidence for an intermediate state from infrared spectroscopy. J Phys: Condensed Matter 12:5189-5199
Zhang M, Salje EKH, Farnan I, Graeme-Barber A, Daniel P, Ewing RC, Clark AM, Leroux H (2000b) Metamictization of zircon: Raman spectroscopic study. J Phys: Condensed Matter 12:1915-1925
Zhang M, Salje EKH, Capitani GC, Leroux H, Clark AM, Schlüter J, Ewing RC (2000c) Annealing of α-decay damage in zircon: a Raman spectroscopic study. J Phys: Condensed Matter 12:3131-3148
Zhang M, Salje EKH (2001) Infrared spectroscopic analysis of zircon: Radiation damage and the metamict state. J Phys: Condensed Matter 13:3057-3071
Zhang M, Salje EKH, Ewing RC (2002) Infrared spectra of Si-O overtones, hydrous species, and U ions in metamict zircon: radiation damage and recrystallization. J Phys: Condensed Matter 14:3333-3352
Ziegler JF, Biersack JP, Littmark U (1985) The Stopping and Range of Ions in Solids. Pergamon, New York.
Ziegler JF (2002) http://www.SRIM.org/
Zinkle SJ, Kinoshita C (1997) Defect production in ceramics. J Nucl Mater 251:200-217F